

Article

Daily Area of Snow Melt Onset on Arctic Sea Ice from Passive Microwave Satellite Observations 1979–2012

Angela C. Bliss * and Mark R. Anderson

Earth and Atmospheric Sciences, University of Nebraska-Lincoln, 214 Bessey Hall Lincoln, NE 68588-0340, USA; E-Mail: mra@unl.edu

* Author to whom correspondence should be addressed; E-Mail: acbliss3@huskers.unl.edu; Tel.: +1-402-472-2663; Fax: +1-402-472-4917.

External Editors: Rosa Lasaponara and Prasad S. Thenkabail

Received: 6 August 2014; in revised form: 6 October 2014 / Accepted: 24 October 2014 /

Published: 13 November 2014

Abstract: Variability in snow melt onset (MO) on Arctic sea ice since 1979 is examined by determining the area of sea ice experiencing the onset of melting during the melt season on a daily basis. The daily MO area of the snow and ice surface is determined from passive microwave satellite-derived MO dates for the Arctic Ocean and sub-regions. Annual accumulations of MO area are determined by summing the time series of daily MO area through the melt season. Daily areas and annual accumulations of MO area highlight inter-annual and regional variability in the timing of MO area, which is sensitive to day-to-day variations in spring weather conditions. Two distinct spatial patterns in MO area accumulations including an intense, fast accumulating melt area pattern and a slow accumulating melt pattern are examined for two melting events in the Kara Sea. In comparing the 34 years of MO dates for the Arctic Ocean and sub-regions, melt accumulations have changed during the period. In the earlier years, 1979–1987, the MO generally was later in the year than the mean, while in more recent years, the MO accumulations have been occurring earlier in the melt season. The sub-regions of the Arctic Ocean also exhibit greater annual variability than the Arctic Ocean.

Keywords: Arctic; sea ice; melt onset; snow melt; passive microwave; remote sensing

1. Introduction

Arctic sea ice is varying rapidly and is a sensitive indicator of climate change. Over the satellite record, Arctic sea ice thickness and annual extent minima have seen drastic reductions. The 2012 sea ice extent minima of 3.4×10^6 km² reached on 13 September 2012 [1] exceeds the previous record set in 2007 by 0.2×10^6 km² on 14 September 2007 [2]. Research shows that declining sea ice thickness [3,4] leaves the ice cover more susceptible to melt forcing conditions such as anomalous winds advecting sea ice away from the coast and increased ice transport out of the Arctic [2,5,6]. Preconditioning of the ice cover (e.g., reduction in overall sea ice volume and loss of multiyear ice, increased proportion of thin, seasonal ice, *etc.*) [2] leaves the sea ice more vulnerable to episodic melting events during the summer such as occurred during “The Great Arctic Cyclone of August 2012,” coined by Simmonds and Rudeva [7].

Due to the complexities of mechanisms contributing to the declining Arctic sea ice, a direct correlation between the date of melt onset on the sea ice surface and summer sea ice extent has not been found [8]. However, the timing of the annual onset of melting of snow and ice plays a role in summer sea ice reductions via the ice-albedo feedback loop [9]. The timing of melt onset in the Arctic is an important control for the amount of solar radiation absorbed by the ice-ocean system throughout the melt season [10]. The albedo reduction associated with the onset of melting in the snow cover atop sea ice during the spring and early summer increases the absorption of solar radiation [11]. Following an initial reduction in snow albedo, melt ponds form and seasonal ice melts completely allowing more radiation to be absorbed throughout the season [12]. Increased absorption leads to delays in freeze-up and the continued thinning of the ice volume, compounding the loss of sea ice in the following years. The date on which melting atop sea ice begins in the spring is exceedingly important. The balance of higher incident solar radiation in spring and early summer with reduced sea ice concentrations resulting from melting in the ice pack maximizes the effects of the ice-albedo feedback loop [9,10,13]. Since solar radiation in the Arctic gradually tapers off through the summer months, the timing of freeze-up in the fall does not impact the next year’s ice conditions to the same extreme that early melt onset can influence the annual September sea ice extent minimum for the current year [10,13].

Several algorithms utilizing passive microwave satellite data exist to determine the timing of melt onset on sea ice (e.g., [13–17]). Passive microwave derived melt onset dates are preferred to active microwave or combination active and passive microwave melt onset dates for this research because of the largely consistent record of passive microwave brightness temperatures dating from 1979 through 2012. The day on which melt onset occurs is closely associated with near-freezing air temperatures. The onset of melting is a sensitive indicator of the near-surface atmospheric conditions, particularly the air temperature; therefore the timing of melt onset can give information directly related to the larger scale weather conditions present at the time of melt [18].

Variations in the onset of melting through the satellite record can indicate differences occurring in spring weather systems [8,13,19]. In addition to inter-annual variability, there is high regional variability in the onset of melting in the Arctic [13,14,18]. Sub-regions within the Arctic have highly variable melt onset timing which is largely independent of the melt onset timing of other regions during a given year [18]. This is likely due to variations in local atmospheric conditions and differences in geography for locations across the Arctic. For example, a region with open water (*versus* land or ice-locked area)

upwind of the region of interest can influence the timing of melting due to the availability of ocean heat flux in ice-free ocean regions [18,20].

Detailed information about the timing of melting on the sea ice surface can be gained by partitioning an annual map of melt onset dates into a daily area of pixel locations undergoing melt, first described by Bliss and Anderson [21]. Here we examine the onset of melting on a daily basis in terms of area for the years 1979–2012 and identify differing characteristics in the timing and magnitude of melt onset events that result in the accumulation of springtime melting areas across the sea ice surface. Given the high regional variability of the timing of melt onset due to weather conditions present at the time of melting, we identify the spatial and temporal patterns in melt onset for the Arctic Ocean as a whole and sub-regions within the Arctic Ocean. We find that melt onset area is accumulating increasingly early in the year over much of the Arctic sea ice cover and the spatial and temporal patterns in daily melt onset area may give insight into changes in spring weather conditions occurring at the time of melt onset.

2. Data

The melt onset dates used here are from the Snow Melt Onset Over Arctic Sea Ice data set distributed by the National Snow and Ice Data Center (NSIDC) in Boulder, CO [22]. The data are formatted in the Northern Hemisphere polar stereographic grid (304×448 pixels) with a resolution of 25 km available from NSIDC [23]. The melt onset dates are available as an annual, gridded array giving the day from the first of the year (DOY) on which melting began for each year of the data record [22]. The melt onset dates are determined for each year beginning 1 March through the beginning of September. 1 March usually corresponds with the timing of maximum Arctic ice extent following the winter freeze-up period and early September marks the end of the melt season when sea ice extent nears its annual minimum [1,22].

Melt onset dates are calculated using the Advanced Horizontal Range Algorithm (AHRA) developed by Drobot and Anderson [15]. The algorithm utilizes the range between horizontally polarized, daily brightness temperatures (Tbs) from multiple passive microwave satellite platforms. Melt season Tbs used to calculate the AHRA melt onset dates were collected by the Scanning Multichannel Microwave Radiometer (SMMR) on board the NASA Nimbus 7 platform every second day beginning in late 1978 through 1987 and daily for the years 1988–2012 with the Special Sensor Microwave Imagers (SSM/I) and Sounder (SSMIS) on board the Defense Meteorological Satellite Program's F08, F11, F13, and F17 platforms. Before the AHRA is applied to the Tbs, data from each sensor are calibrated through time using linear regression coefficients determined from data overlap periods. This adjustment is done to create a consistent record of Tbs throughout the 34 year study period. The linear regression coefficients are applied using F08 as the baseline platform [24–27].

The AHRA calculates the difference between the 19 GHz (18 GHz for SMMR) and 37 GHz horizontally polarized Tbs (see Drobot and Anderson [15] for details on the algorithm). A distinctive change in the Tb occurs when liquid water becomes present atop sea ice due to the high emissivity of liquid water surrounding snow grains. When melt onset is detected, the algorithm assigns the DOY on which this melting signature first occurs at each grid point location. The AHRA is designed to be insensitive to short term weather effects and spurious Tbs by testing within a 10-day time series on either side of the date being examined. The 10-day time series is used to verify that a change in the Tbs is due

to a change in the snow and ice surface, indicating melt, rather than effects of weather interference in the passive microwave Tbs such as liquid water clouds [15].

The AHRA algorithm works for both multi-year and first year sea ice locations [15]. The range between 19 and 37 GHz channel Tbs remains positive during wintertime conditions over multi-year ice due to the greater emissivity at 19 GHz and increased volume scattering at 37 GHz. Over first year ice, the range between the 19 and 37 GHz Tbs is much smaller than over multi-year ice because the emissivities at 19 GHz and 37 GHz are similar for first year ice during winter conditions [15]. A melt onset date can be assigned when the difference between the 19 GHz and 37 GHz channel Tbs is 4.0 K or less. The Tb range for first year sea ice during winter conditions can dip below this threshold, however, they recover quickly to values above the 4.0 K threshold [15]. The 10-day time series described above prevents the algorithm from assigning first year ice locations with a melt onset date that is too early, before air temperatures reach 0 °C.

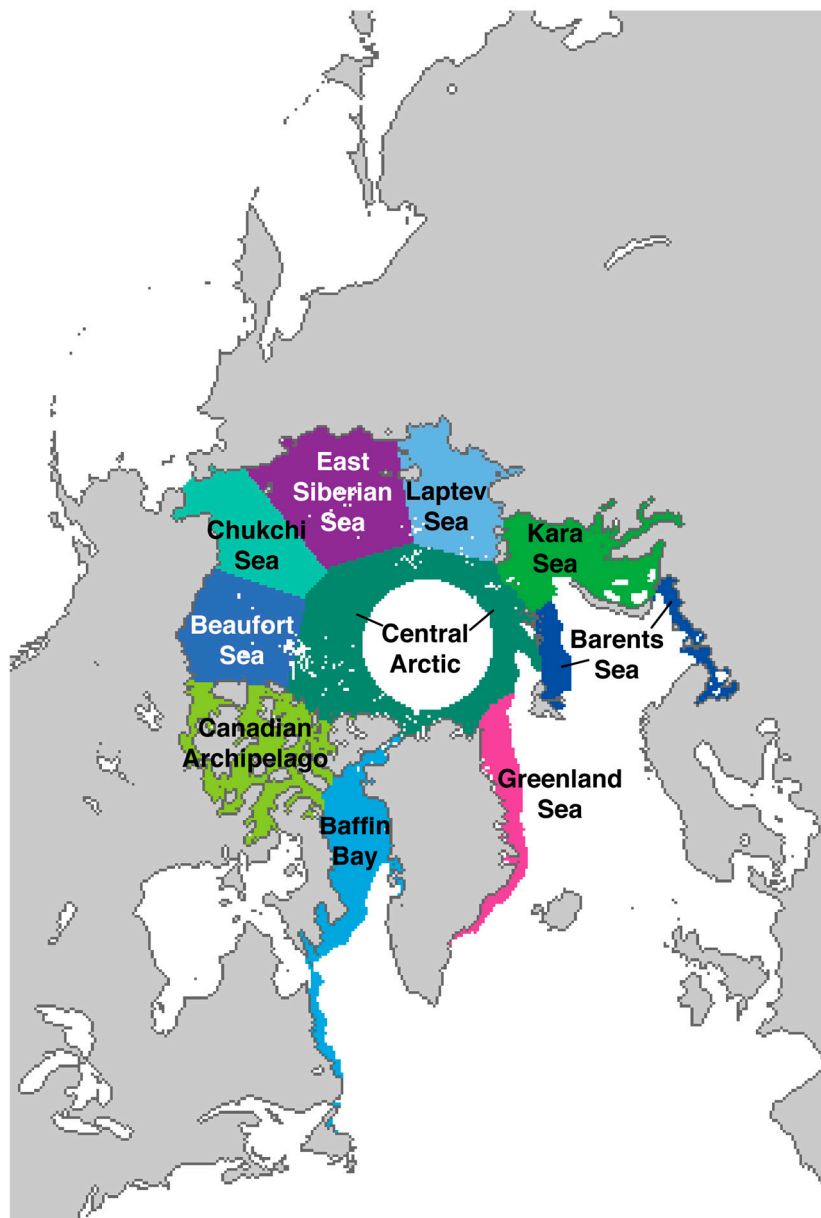
The melt onset dates from the AHRA are comparable to the beginning of the “early melt” period defined by Livingstone *et al.* [28] and used by Markus *et al.* [14]. “Early melt” corresponds to the period of time during which maximum daily temperatures reach the freezing point, however, the snow and ice cover may continue to melt and refreeze as diurnal temperatures cycle above and below freezing.

3. Methods

We describe inter-annual and regional variability of melt onset on a daily basis by examining the AHRA melt onset dates for the melt seasons of 1979–2012. Regional variations in the timing of MO area are high and are dependent on both latitude and variations in atmospheric circulation [15]. Therefore, we divide sea ice locations in the Arctic into common geographic regions that are comparable to those of other studies (*i.e.*, [14,29,30]). We primarily focus our regional analysis on sub-regions within the Arctic Ocean and Baffin Bay where inter-annual variation in the timing of MO is high. For this study, we use the term Arctic Ocean to represent the Barents, Kara, Laptev, East Siberian, Chukchi, and Beaufort Seas, the Canadian Arctic Archipelago, the Central Arctic, Baffin Bay, and the Greenland Sea (all sub-regions indicated on Figure 1). Sea ice-covered locations outside of these regions are excluded from this study because slight outliers in MO area can greatly dominate statistics due to the smaller ice-covered areas within the regions. Additionally, air temperatures are generally warmer in these southerly locations and the accumulation of MO area occurs much more quickly and earlier in the year than for most land-locked regions at higher latitudes and within the Arctic Ocean; thus there is comparatively little variation in MO timing from year to year.

The mean MO date and standard deviation of the MO dates for each region are calculated from pixel points within each defined region where a MO date exists for all 34 years in the study period. The mean range of MO dates is the difference between the latest mean MO date and the earliest MO date for each region.

Figure 1. Map illustrating sea ice locations used in analysis. Colored pixels indicate locations where a melt onset date exists for all 34 years in the study period. White pixels represent fewer than 34 years of data within a region and were not included in the analysis. Different colors distinguish the boundaries between sub-regions within the Arctic Ocean.



To determine daily area of MO, for each day of the melt season after 1 March (DOY 60), the number of grid point locations with a melt date assigned for each day is multiplied by the grid resolution ($25 \text{ km} \times 25 \text{ km}$) to produce the area of sea ice experiencing melt onset (MO) for that date. Hereafter, this value is referred to as the daily MO area. A time series of daily MO area throughout a single melt season is used to determine the timing and magnitude of individual melting events within a defined region. Here we define a “melting event” as a period of time over which large areas of MO occur for several consecutive days. For days prior to and immediately following a melting event, the daily MO area is 0 km or near 0 km per day. Although the total duration of a melting event can vary from a few days to a month or more, MO area during the event is large resulting in MO for 50% or more

of a region's geographical area. The passive microwave data used in this study have different temporal coverage; SMMR data from 1979 to 1987 were only generated every second day, while data collected since 1988 were generated daily. Thus, a 3 day running mean is applied to the time series of daily MO areas for each year to make the daily MO areas before 1988 more comparable to daily SSM/I and SSMIS data. The running mean can slightly smooth the daily MO area curves and can shift the apex of a peak in the curve (a local maximum MO day) ± 1 day. For the purposes of this work in illustrating the usefulness of daily MO area analysis, we show the daily MO areas for each year in the Kara Sea only. However, data for the Arctic Ocean and other sub-regions discussed in this work are provided in the Supplementary Figures S1–S10.

In addition to the time series of daily MO areas, we map the pixel locations experiencing MO for two melting events in the Kara Sea on a daily basis and relate the melting events with the atmospheric conditions present at the time of melt. A daily map of MO pixel locations within a sub-region visually represents the spatial progression of MO area across an area of the sea ice for a period of time. Since MO area can occur at each grid point location only once per year, there is a decreasing utility of daily MO area in identifying the magnitude or intensity of melting events that occur later in the melt season, simply because there are fewer grid points remaining that can be considered new MO areas. Given this limitation, valuable information can be gained by closely examining patterns in the daily MO areas, especially variations in the regional MO pattern from year to year. Thus, we examine melting events that cover only the first 90% of a region. Finally, we show annual accumulations of MO area for each year. Annual accumulations are calculated by summing the time series of MO areas for each day through the melt season.

To ensure that the daily MO area and annual MO area accumulations are directly comparable from year to year, MO area is only calculated over grid points where a MO date exists for all 34 years of the record (identified in Figure 1 by colored pixels). Therefore, pixels with less than 34 years of melt (white pixels in Figure 1) are excluded from this analysis. The total area of sea ice coverage (km^2) for the Arctic Ocean and its sub-regions are presented in Table 1. Note that the white circle centered over 90°N latitude and within the Central Arctic sub-region corresponds to the pole hole (Figure 1), an area where no data are collected by the passive microwave sensors due to the orbiting paths of the satellites. Since Tb data from SMMR were collected every second day, accumulation curves for 1979–1987 are not smooth, instead having a stair-step appearance. Although not as smooth as curves in later years of the record, the annual curves for SMMR years are comparable to annual MO accumulations for the other years in the record. Melting events that occur early in the melt season lessen the magnitude of melting events occurring later in the melt season because MO occurs exactly once per year for sea ice locations. The day on which 50% MO area occurs is used as a representation of the median of the time period over which MO area accumulates across all sea ice area. We group SMMR data separately to avoid confusion regarding data inconsistencies. Hereafter, daily MO area plots and MO area accumulation curves for each region are divided into 3 time periods: (a) SMMR 1979–1987, (b) early SSM/I 1988–1999, and (c) late SSM/I and SSMIS 2000–2012 for better visualization. The mean MO accumulation curve and range of accumulations for 1979–2012 are the same across the three time periods defined above.

Table 1. Melt onset date summary statistics 1979–2012.

Region	Region Area (10 ⁵ km ²)	Mean MO Date (DOY)	Mean Standard Deviation (Days)	Mean Range (Days)
Arctic Ocean	87.5	22 May (141.9)	8.7	30.4
Barents Sea	3.5	4 April (93.9)	12.2	52.2
Kara Sea	8.3	11 May (130.5)	12.8	54.0
Laptev Sea	8.4	25 May (144.9)	11.7	51.2
East Siberian Sea	12.6	31 May (150.1)	14.5	47.4
Chukchi Sea	8.2	17 May (136.3)	12.7	48.0
Beaufort Sea	9.0	28 May (148.0)	9.9	35.2
Canadian Archipelago	7.4	29 May (149.0)	7.7	32.2
Central Arctic	17.9	10 June (160.9)	9.5	37.7
Baffin Bay	8.2	1 May (120.6)	10.0	35.2
Greenland Sea	4.0	29 April (118.9)	11.1	38.7

4. Typical Variability in Melt Onset Dates

For the Arctic Ocean region, the mean MO date is 22 May (DOY 141.9) with a standard deviation of ± 8.7 days (Table 1). The range of annual mean MO dates is 30.4 days indicating that the average MO date varies within the 34-year record by approximately 1 month. The sub-regions of the Arctic Ocean are more highly variable. The mean ranges for sub-regions vary from 32.2 days in the Canadian Archipelago to 54 days in the Kara Sea (Table 1). The mean MO dates for sub-regions is indicative of the geographic and latitudinal controls on the timing of MO. The Barents Sea has the earliest mean MO date on 4 April (DOY 93.9). The ice extent in the Barents Sea region that is consistent in all 34 years of the MO record (Figure 1) is also small (3.5×10^5 km²) relative to the sea ice region areas of other sub-regions. The large proportion of open ocean within the Barents Sea can contribute to the earlier mean MO date observed due to the availability of ocean heat flux source from the open water areas.

In contrast, the latest mean MO date occurs on 10 June (DOY 160.9) in the Central Arctic region (Table 1). The Central Arctic region has the highest latitudes, surrounding the pole, thus MO typically occurs latest. The region that is least variable from year to year (defined by the lowest standard deviation of ± 7.7 days) is the Canadian Arctic Archipelago, which has a mean MO date of 29 May (DOY 149) (Table 1). This region contains the highest proportion of multi-year ice and is largely landlocked, with little open water during the spring [3]. Thus, the typical MO timing in this region is much later than regions that are primarily covered in thin, seasonal ice.

The most highly variable MO dates occur in other regions within the Arctic Ocean including the Kara, Laptev, East Siberian, and Chukchi Seas. Mean MO dates in these regions range from 11 May (DOY 130.5) in the Kara Sea to 31 May (DOY 150.1) in the East Siberian Sea (Table 1). The largest mean range in MO dates (54 days) occurs in the Kara Sea. The Kara Sea mean MO range indicates that the mean MO date varies by nearly 8 weeks over the 34 year record, making the Kara Sea the most highly variable sub-region of the Arctic Ocean. Since the Kara Sea and other Arctic Ocean sub-regions are highly variable in terms of MO timing from year to year, MO timing is attributed to the large-scale weather patterns, in particular, cyclonic activity present at the time of MO [18]. The patterns of daily MO in these regions can point to the ideal atmospheric conditions necessary to initiate the onset of

melting over large proportions of a region's area. For these reasons, we primarily focus the discussion of daily MO events on the highly variable Kara Sea region and provide plots for the other Arctic Ocean regions.

5. Daily Melt Onset Areas

5.1. Timing and Magnitude of Melt Onset Events

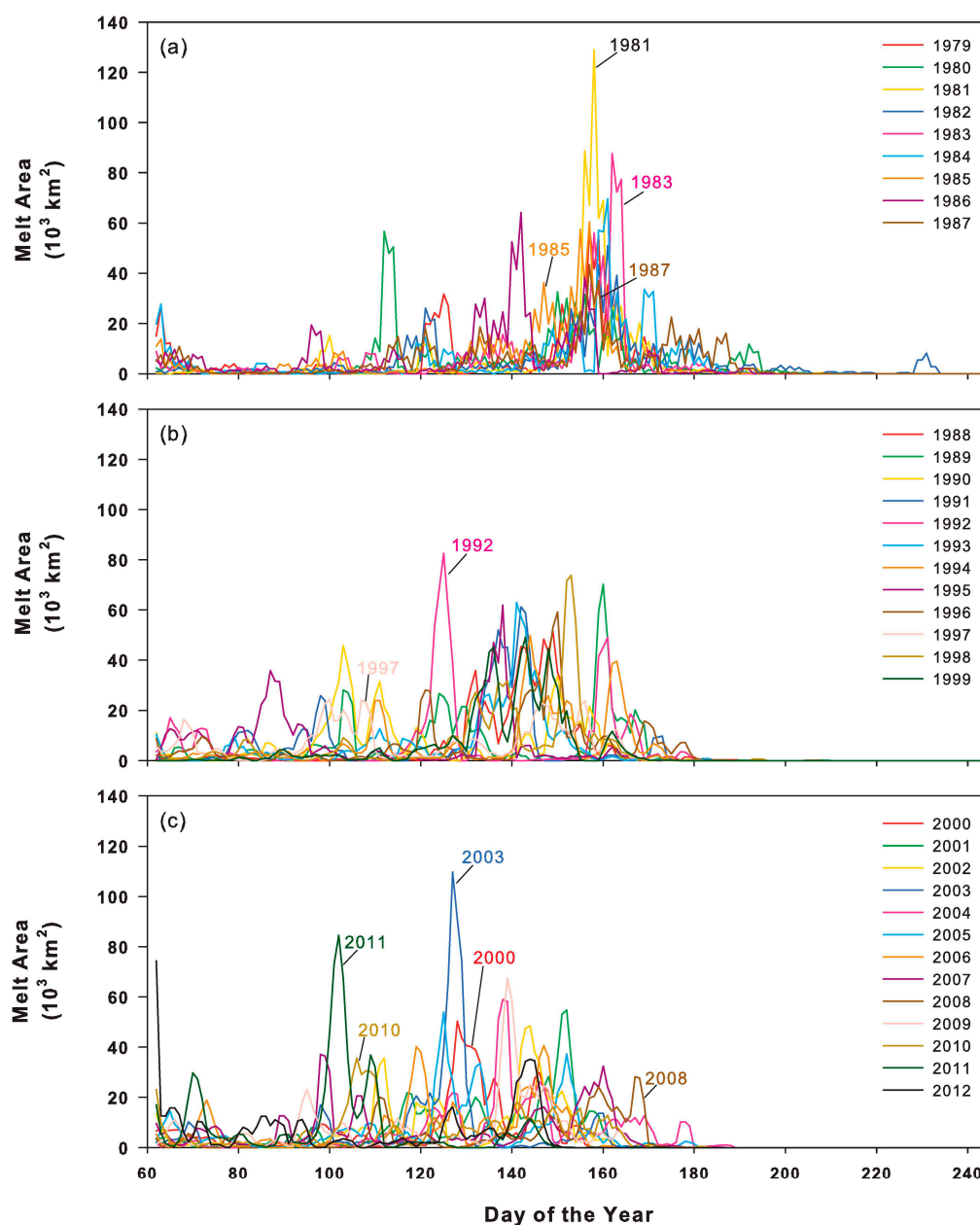
To illustrate the daily MO area timing, 3 day averaged daily MO area curves for the Arctic Ocean and sub-regions were calculated (Figure 2 and Supplement Figures S1–S10). In all regions, similar variations in the individual MO area curves exist and different patterns can be identified in different years. For example, there are large areas of melt which occur over very short periods of time, represented by large peaks in the 3 day averaged MO areas, vs. small areas of melt over the same time period (see Figure 2). The timing for when these large areas of melt occur during the melt season indicates an early or delayed MO signal for each region. The strength or track of the atmospheric weather system forcing the onset of melting over a region area can also affect the size of the peak of melting area where very intense melt conditions produce larger areas of MO. The regional and temporal variability of MO across the regions and the sensitivity of the timing of MO area accumulations are most likely due to the daily weather conditions during melt. Further analysis of the MO area patterns in each region and the direct relationship to the atmospheric conditions is necessary to thoroughly explain the causes of the variability in daily MO area at a large scale. A full description of atmospheric conditions during each melt event are beyond the scope of this paper and will be published separately, however, we do illustrate the atmospheric conditions during two different melting events for the Kara Sea using data from the NCEP/NCAR Reanalysis [31]. Here we primarily focus on the magnitude and timing of peaks in the MO area time series and how the variability compares within a region and between regions. In general, there is a shift in the dates when the largest peaks occur within a region. Most regions have larger melt events later in the year in the SMMR years, while the more recent years, SSM/I and SSMIS data have the large melt events earlier in an individual year.

5.2. Melt Onset Event Case Study: Kara Sea

We illustrate the usefulness of an analysis of the daily MO area here by describing details in the Kara Sea region, which has the highest inter-annual variability in MO area accumulation in terms of MO area range (Table 1). Peaks in the annual 3 day averaged MO area indicate the timing and magnitude of melting events for the Kara Sea (Figure 2). The largest peaks indicate intense melting where large areas of the sea ice within the region are experiencing MO. In this type of event, the largest daily MO areas typically accumulate over 3–5 consecutive days. Some examples of this type of melting event are seen in years such as 1981, 1983, 1992, 2003, and 2011 (Figure 2). The greatest MO day in the Kara Sea, occurs on DOY 158 1981 on which 1.34×10^5 km² of the region area experienced MO. The second greatest MO peak occurs on DOY 127 2003 on which 1.16×10^5 km² experienced MO and the third greatest MO peak occurs on DOY 162 1983 on which 0.92×10^5 km² of the region begins to melt. Given that the mean MO date for the Kara Sea occurs on 11 May (DOY 131, Table 1) it is interesting to note that the peak MO days in 1981 and 1983, occur approximately 30 days after the mean MO day

(DOY 131), while the peak melting day in 2003 (DOY 127) occurs near the mean MO day. An overall tendency towards earlier MO is apparent because of the early 2003 peak day relative to the peak days in 1981 and 1983; however, the magnitude of MO area in 2003 is not greater or dissimilar to the magnitude of large melting events in the 1980s. The melting event in 2003 does, however, occur earlier in the year than either of the 1980s peak events. It should be noted that a 7-day data outage occurs through 19–25 March 2008. $3.06 \times 10^5 \text{ km}^2$ (35% of the Kara Sea area) experienced MO immediately following this period, but due to the data outage and the 10 day window used to calculate MO in the AHRA, the timing of this melted area cannot be fully resolved and is omitted from Figure 2c.

Figure 2. Kara Sea 3 day running mean of daily melt onset (MO) area for (a) Scanning Multichannel Microwave Radiometer (SMMR) years; (b) early SSM/I years; and (c) late SSM/I and SSMIS years.



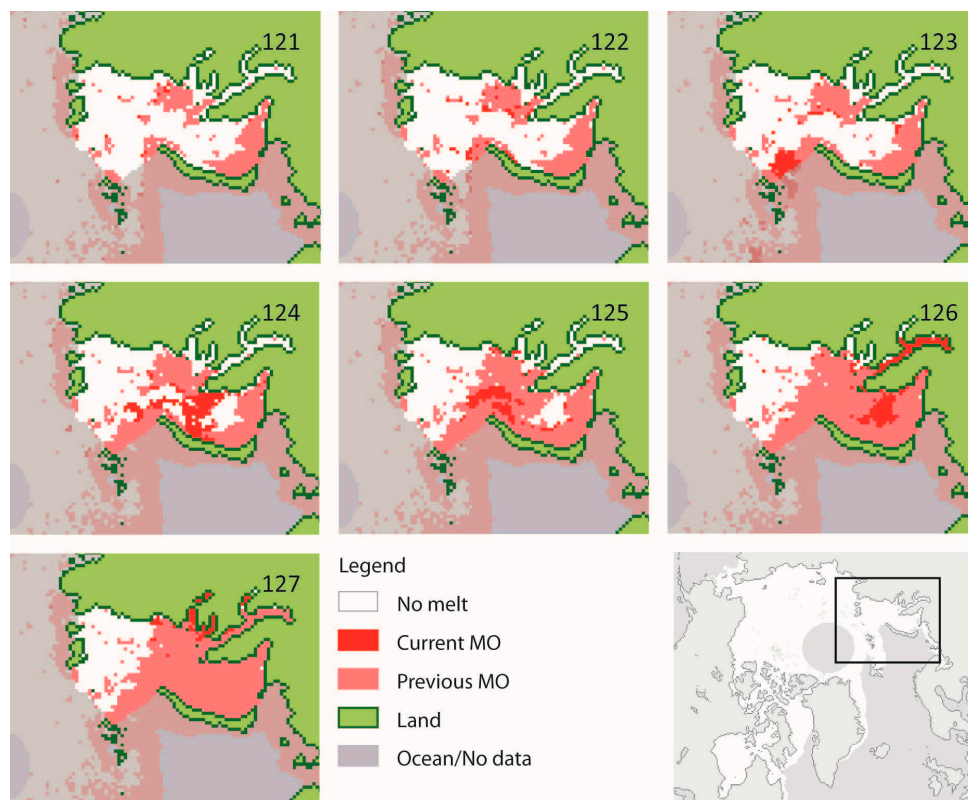
Peaks in MO area as large as a magnitude that occurred in 1981, 1992, and 2003 do not occur every year. There are some cases where the MO area accumulates slowly over a longer time period. These events appear as a shorter, wider peak in the daily MO area time series such as occurs for 1985, 1987, 1997, 2000, and 2010 in the Kara Sea region (Figure 2). Although the accumulation of MO area occurs slowly, these melting events are generally responsible for the onset of melting over nearly the entire area. In cases such as these, it is assumed that the weather conditions are different from conditions that occur with the larger, intense MO area peaks. The largest peaks are likely the result of strong cyclonic activity where widespread warm temperature anomalies exist while years where no large peaks exist are likely the result of cooler temperatures associated with decreased cyclonic activity, leading to delayed accumulations of MO area.

To further examine the spatial character of the accumulations of MO area in both melting event types, two representative example cases were chosen from the Kara Sea. An example of the first type of MO event; a tall, narrow peak, in the Kara Sea occurs in 1992 and is associated with the peak spanning DOY 121–127 (Figure 2b). The second MO event type; a shorter, wider peak, is represented by the event spanning DOY 130–164 in 1985 (Figure 2a). Daily mapping of the locations experiencing MO through the duration of these example events shows the spatial progression and accumulation of MO over a large proportion of the sea ice cover in the Kara Sea. “Current MO” locations indicated with red show pixels that melted on the indicated DOY, while “previous MO” locations indicated in pink show locations that have melted earlier in the year and just prior to the currently mapped date. White pixels show sea ice locations that have not yet melted or will melt at a later date. We include MO information for sea ice locations adjacent to the Kara Sea, but use shading to de-emphasize the MO locations occurring outside of the region boundary.

5.2.1. Kara Sea 1992

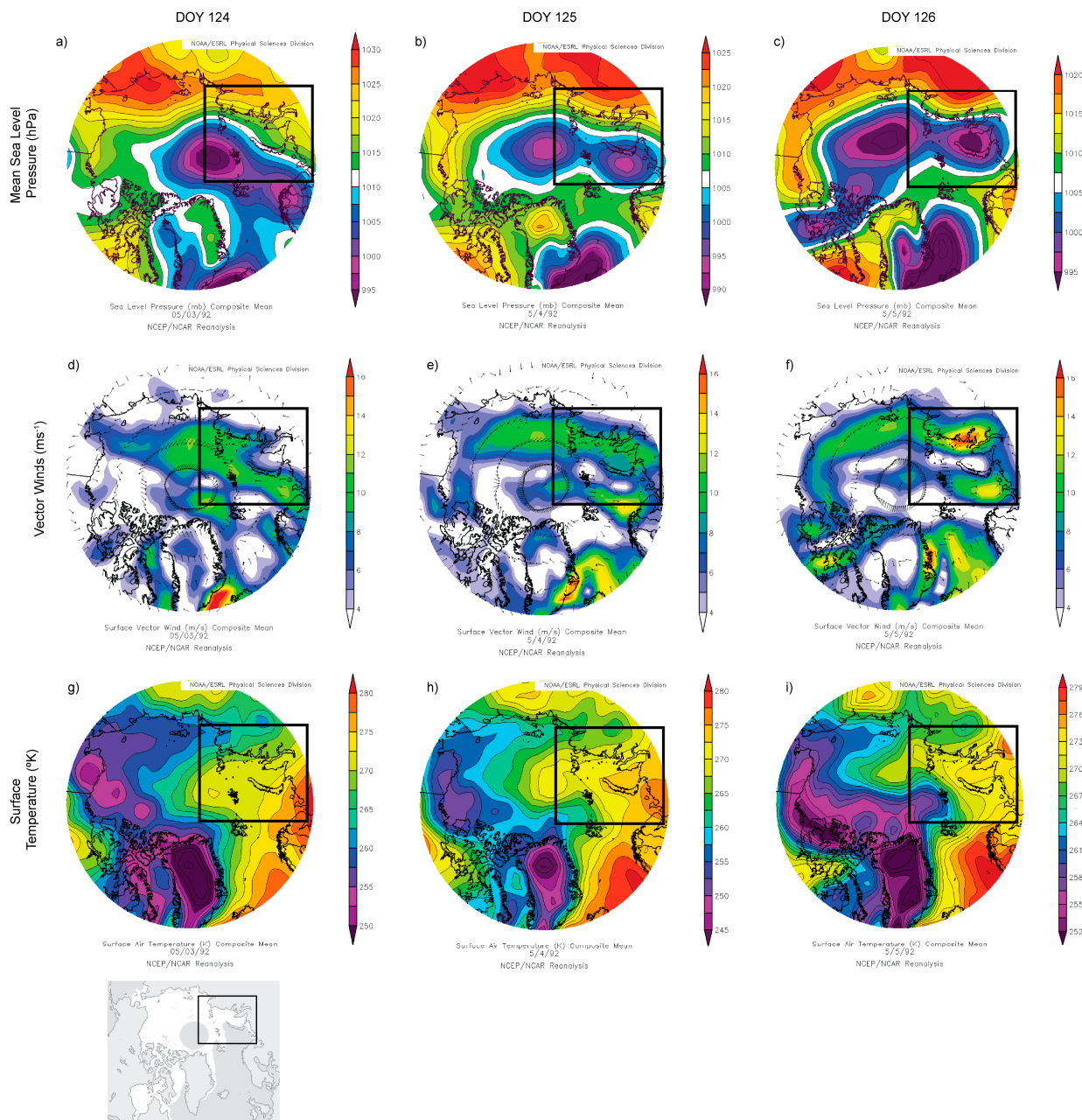
The largest, intense peak in MO area for the Kara Sea in 1992 begins in May, with the greatest MO area day occurring on DOY 124. Prior to this peak MO day, MO area accumulates slowly on DOY 121–122 (Figure 3). MO is observed at only 14 pixel locations on DOY 121 ($0.09 \times 10^5 \text{ km}^2$) and 41 pixel locations on DOY 122 ($0.3 \times 10^5 \text{ km}^2$). On DOY 123, however, the number of pixels, with MO begins to increase. DOY 124 is the peak melting day with the majority of the Kara Sea (168 pixels, $1.05 \times 10^5 \text{ km}^2$) being melted on this day. MO area continues to accumulate quickly through DOY 125–126 before slowing on DOY 127. During this melt event, the majority of the MO area accumulates between DOY 123 and DOY 127. Not only is the MO area accumulation for this event occurring over just a few days, but the melted area fills in locations adjacent to those that have previously melted and is primarily restricted to the southwestern portion of the region. In total, this 5 day melting event accounts for $3.37 \times 10^5 \text{ km}^2$ of MO area or 39% of the Kara Sea’s total area. The time frame and spatially adjacent nature of MO area accumulations horizontally across the ice surface indicate that the melting across several days is the result of strong cyclonic forcing.

Figure 3. Progression of Kara Sea MO area for DOY 121–127 1992. MO locations for the current DOY and where MO has already occurred on a previous day are highlighted. Pixels outside of the Kara Sea region (see Figure 1) are de-emphasized to indicate MO conditions adjacent to the Kara Sea.



During this event, the daily averaged mean sea level pressures (MSLP), surface air temperatures, and wind vectors from the NCEP/NCAR Reanalysis data shown in Figure 4 [32] indicate that a cyclone is present in the Kara Sea region during this melting event [31]. On the peak melting day (DOY 124) an area of low pressure, located to the southwest of the Kara Sea and centered over northern Norway, develops (Figure 4a) and during the next two days approaches and passes over the Kara Sea (Figure 4b,c). The position of this cyclone results in a southerly wind direction within the Kara Sea (Figure 4d,e) on days 124–125 and increasing air temperatures (Figure 4g,h,i). During this three-day period, the 273 °K isotherm advances over the Kara Sea region from the southwest (Figure 4d,e,f) indicating the advection of warmer air temperatures from the south. The melting pattern seen over the southwestern Kara Sea during this period corresponds with the above freezing temperatures advancing over the sea ice (Figure 3). It is important to note that the air temperatures shown in (Figure 4g,h,i) are the averaged daily surface temperatures. The AHRA algorithm detects the metamorphosis of snow grains when air temperatures reach the freezing point and liquid water becomes present in the snow pack atop the sea ice, however, diurnal temperature fluctuations above and below freezing can still occur after the melt onset date is detected [15]. Thus, daily averaged temperatures above freezing are not necessary to trigger the onset of melting, but rather, the maximum daily temperature must reach the freezing point to initiate melt. In this case, however, the intense melting event over the Kara Sea is related to the presence of a cyclone tracking directly over the Kara Sea, which increased the daily average air temperatures above 273 °K and induced MO over a large portion of the sea ice cover in this region.

Figure 4. Daily average (a–c) mean sea level pressures; (d–f) vector wind directions and magnitude; and (g–i) surface temperatures for DOY 124–126 1992. Boxes define the region surrounding the Kara Sea as shown in Figure 3.



5.2.2. Kara Sea 1985

A shorter, wider peak in the daily MO area curve, the second melting event type, can be characterized during 1985 for the Kara Sea (Figure 2a). The melt accumulation area between DOY 130 and 160 accounts for over 74% ($6.4 \times 10^5 \text{ km}^2$) of the Kara Sea region (Figure 5). It should be noted that MO data in 1985, a SMMR year, are collected every other day due to sensor limitations. The 1985 case occurs later in the year than the 1992 case although more total area begins melt during this event than for the 1992 case. Since the MO area accumulates more slowly over ~ 30 days this type of slow-accumulating MO event is the result of weaker atmospheric forcing. Similar to 1992, new MO area

tends to accumulate at locations adjacent to MO locations from the previous day, showing the progression of MO. The MO area peaks on DOY 156 in 1985 with $1.11 \times 10^5 \text{ km}^2$ of new MO area.

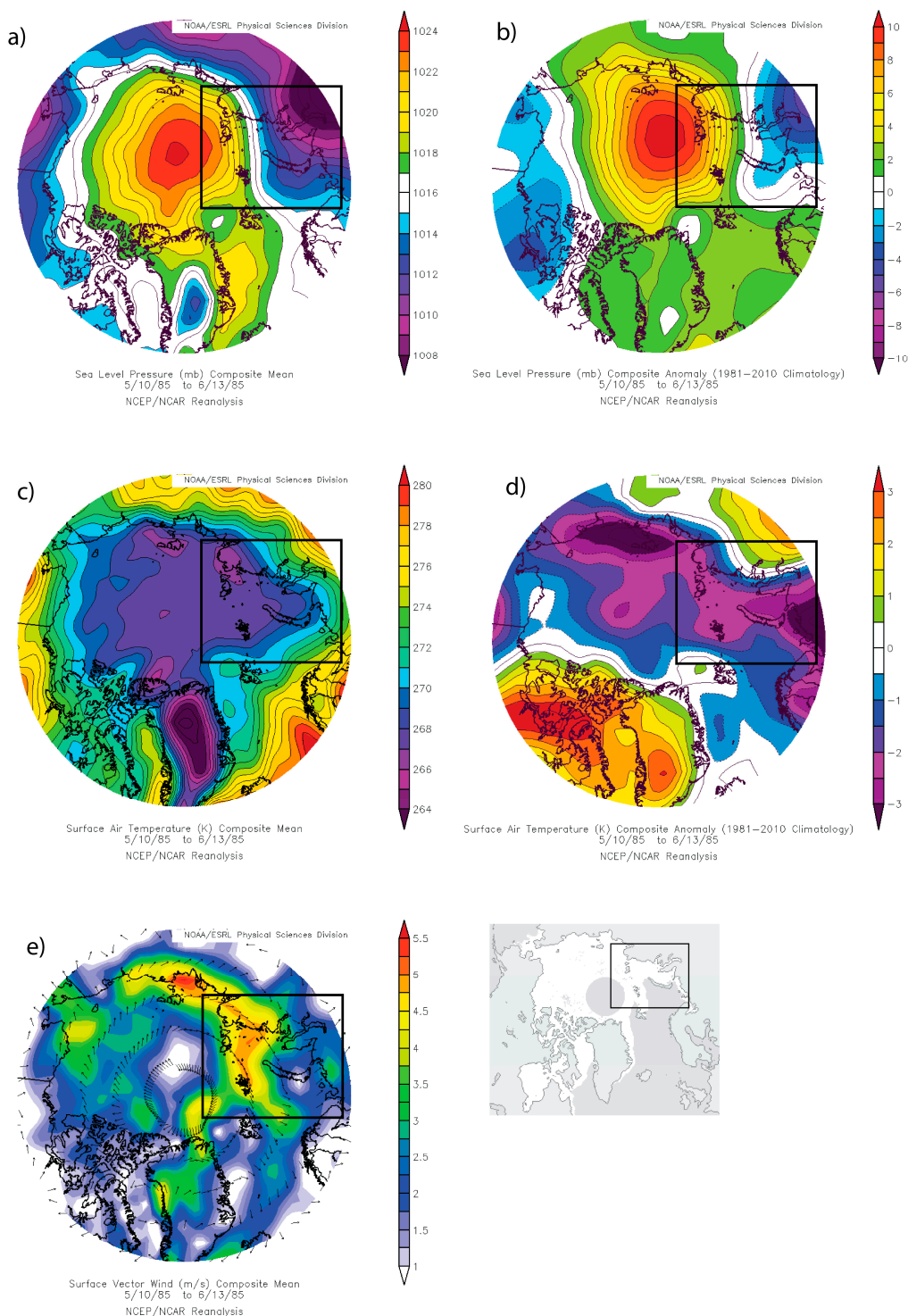
Figure 5. Progression of Kara Sea MO area for DOY 130–164 1985. MO locations for the current DOY and where MO has already occurred on a previous day are highlighted. Pixels outside of the Kara Sea region (see Figure 1) are de-emphasized to indicate MO conditions adjacent to the Kara Sea.



Composite mean atmospheric conditions for the 34 days from DOY 130–164 in 1985 including: MSLP, surface air temperatures, and wind vectors are shown in Figure 6a,c,e [32]. Composite anomalies of MSLP and surface air temperatures relative to the 1981–2010 climate averaging period for the same days in 1985 are shown in Figure 6b,d [32]. The mean atmospheric conditions during the 1985 Kara Sea melting event show near-normal MSLP over the northern portion of the Kara Sea and anomalously low MSLP over the southern Kara Sea and the Ural region of Russia on the continent (Figure 6b). Although low pressures are found adjacent to the Kara Sea during the melt event of 1985, the position of the low pressure area is different from the melting event of 1992 described above. In this case, several transient cyclones do occur during the 34-day period, however, they tend to track to the south of the Kara Sea.

As a result of the mean pressure pattern, the mean wind direction over the Kara Sea tends to be northeasterly (Figure 6e) and surface air temperatures are anomalously cool (Figure 6d).

Figure 6. Composite mean atmospheric (a) mean sea level pressures; (b) sea level pressure anomalies; (c) surface temperatures; (d) surface temperature anomalies; and (e) vector wind directions and magnitude for DOY 130–164 1985. Daily (f) mean sea level pressures are shown for DOY 136 1985. Boxes define the region surrounding the Kara Sea as shown in Figure 5.



One example of a cyclone with a central pressure of less than 985 hPa occurs on DOY 136 (Figure 6f). This cyclone tracks to the south of the Kara Sea, resulting in a northerly wind direction and cooler air temperatures over the region (not shown). Had the track of this cyclone passed over the Kara Sea, warm air advection via southerly cyclonic winds could have produced a more intense, 3–5 day melt onset pattern similar to that which occurred in 1992. The averaged MSLP pattern and resultant low temperature anomaly suppressed the melting during this period in 1985, leading to an extended period of slowly accumulating MO area in the Kara Sea. The spatial pattern in daily MO area shows that MO area in 1985 tends to begin near the coastline and spread towards the northeast towards the central Kara Sea (Figure 5) although temperatures in the region are 2–3 °K below normal (Figure 6d). It is likely that in the absence of a strong cyclonic influence and advection of warmer temperatures like occurs in 1992, increasing latitudinal temperatures during May and early June contributed to the spatial patterns of MO area seen in the Kara Sea during the 1985 melting event.

Due to the heavy reliance of the timing of MO on the local weather conditions present at the time of melt shown for the Kara Sea, we can infer that there may be similarities in the atmospheric forcing occurring at the time of MO in each type of melt event for other regions. Daily MO areas provide detail about the day to day progression of MO across Arctic sea ice within individual years; however, accumulations of MO area throughout the melt season can show the inter-annual variability in these patterns of melt.

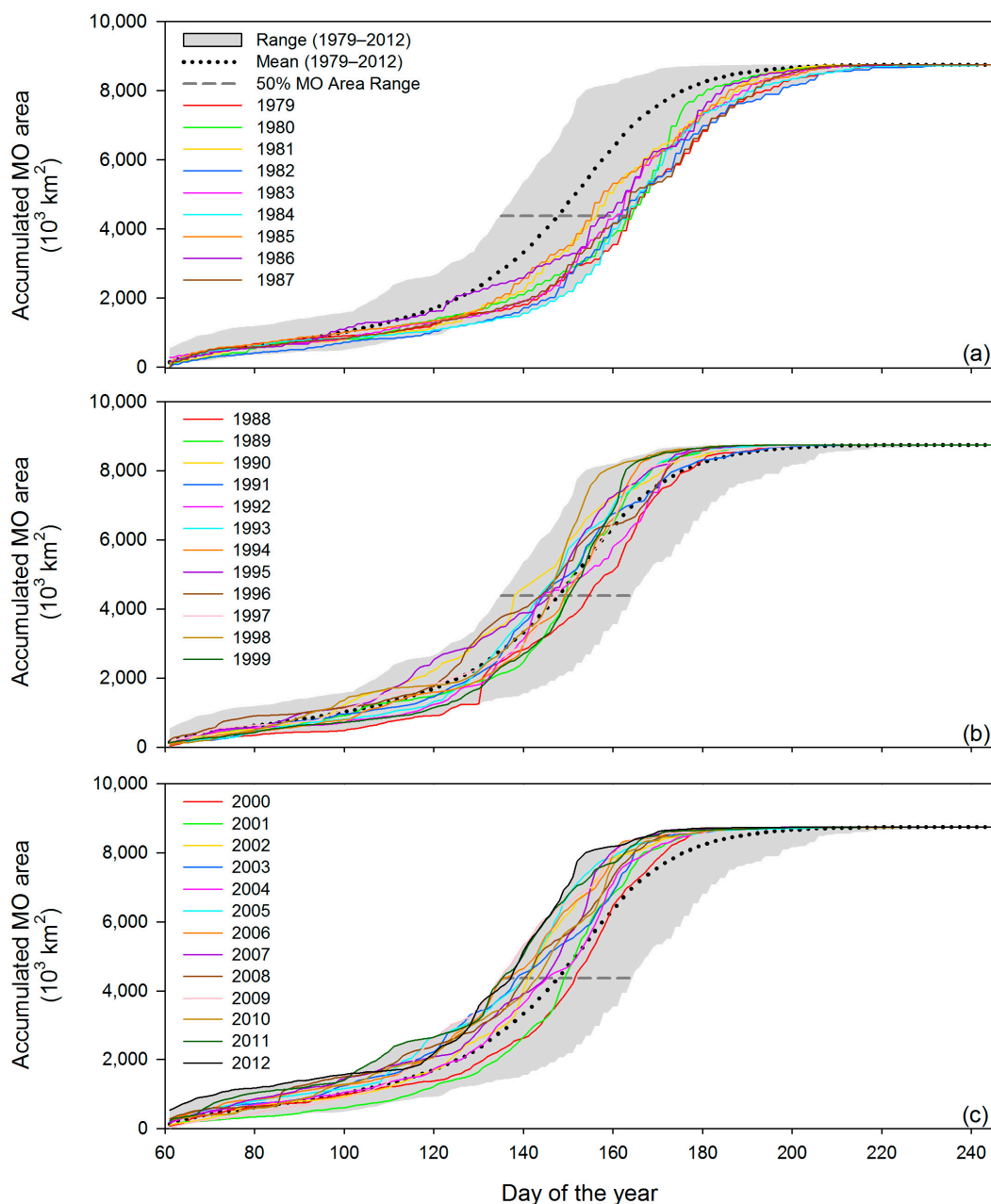
6. Annual Accumulations of Melt Onset Area

Accumulating the daily MO areas throughout the year shows the progression of melting area through a single melt season. The slope of an accumulation curve corresponds to the amount of MO area occurring at a point in time during the melt season. A steep slope indicates a relatively quick accumulation of melting area, while a lower slope indicates a slower accumulation of melting area. Therefore, an intense, large 3–5 day peak would appear as a nearly vertical slope on the annual accumulation, compared to a slow accumulating case represented by a shorter, stair-stepped vertical change.

6.1. Inter-Annual Variability in the Arctic Ocean

Inter-annual variability in the Arctic is evident by the spread of annual MO accumulation curves in Figure 7. A comparison of SMMR years (Figure 7a) to the mean (1979–2012) and range in accumulation across all years (the grey shaded region on each plot) shows that MO accumulation in the early part of the record is different from later years. Since the SMMR years (1979–1987) tend to fall below the mean, MO area accumulates later in the year than average indicating delayed MO relative to other years. The early SSM/I years (1988–1999) have an increased spread when compared to SMMR years and tend to fall both above and below the mean accumulation curve (Figure 7b). Additionally, early SSM/I accumulations do not occupy the bottom of the range after approximately DOY 130. The late SSM/I years (2000–2012) generally fall above the mean, indicating that MO area is accumulating sooner in the year than the mean (Figure 7c). The changes observed in the MO area accumulations for the Arctic Ocean with respect to the mean, describe a change in the MO towards increasingly early melting over large regions of Arctic sea ice.

Figure 7. Arctic Ocean annual accumulated MO areas for (a) SMMR years; (b) early SSM/I years; and (c) late SSM/I and SSMIS years.



The onset of melting causes a reduction in surface albedo of the snow cover atop the sea ice. Earlier reductions in surface albedo increase the amount of solar radiation that can be absorbed by the ice-ocean system throughout the remainder of the melt season. The fact that larger areas of the ice cover are beginning to melt earlier in the season, gives evidence that the surface energy balance in the Arctic is changing. Thus, more solar energy can be absorbed into the region until freeze-up occurs during the autumn. Overall warming air temperatures in the Arctic (e.g., [33–35]) may provide a mechanism for the shift towards earlier MO area accumulations. However, variability in MO area from year to year is also related to the atmospheric circulation patterns and the frequency of cyclonic activity [19]. Due to the scale of cyclonic disturbances, it is also valuable to identify the variations in MO area at the regional scale.

6.2. Variability in Arctic Ocean Sub-Regions

There is considerable regional variability in the annual accumulations of MO area in addition to inter-annual variability for the entire Arctic Ocean. Here, we focus on the sub-regions in the Arctic Ocean (Figure 1). Compared to the relatively smooth “S” shaped accumulation curves for the Arctic Ocean (Figure 7), individual regions of the Arctic Ocean show higher variability in the timing of MO area accumulations from year to year. The pattern of the range of MO area accumulation curves (*i.e.*, the shape of the grey shaded regions of MO area accumulation plots) varies for each sub-region (Figures 8–17). For the purposes of this analysis, the period of time over which MO area accumulates over the total area of a region is referred to as the MO period. It is important to note that the MO period does not refer to the duration of melting at a point location or the local ablation of snow cover, but the duration of time over which a region’s total area experiences the onset of melt following the earliest occurrence of MO for the season.

Figure 8. Barents Sea annual accumulated MO areas for (a) SMMR years; (b) early SSM/I years; and (c) late SSM/I and SSMIS years.

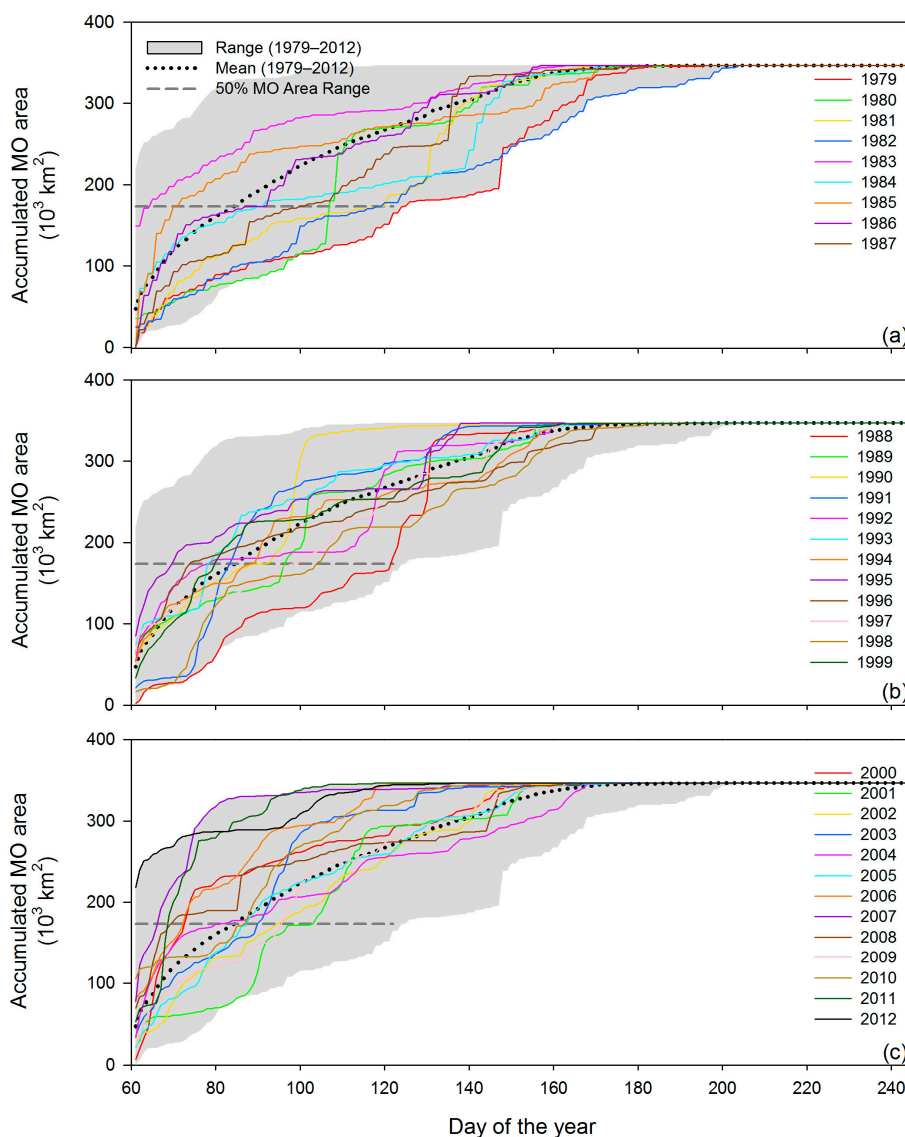


Figure 9. Kara Sea annual accumulated MO areas for (a) SMMR years; (b) early SSM/I years; and (c) late SSM/I and SSMIS years.

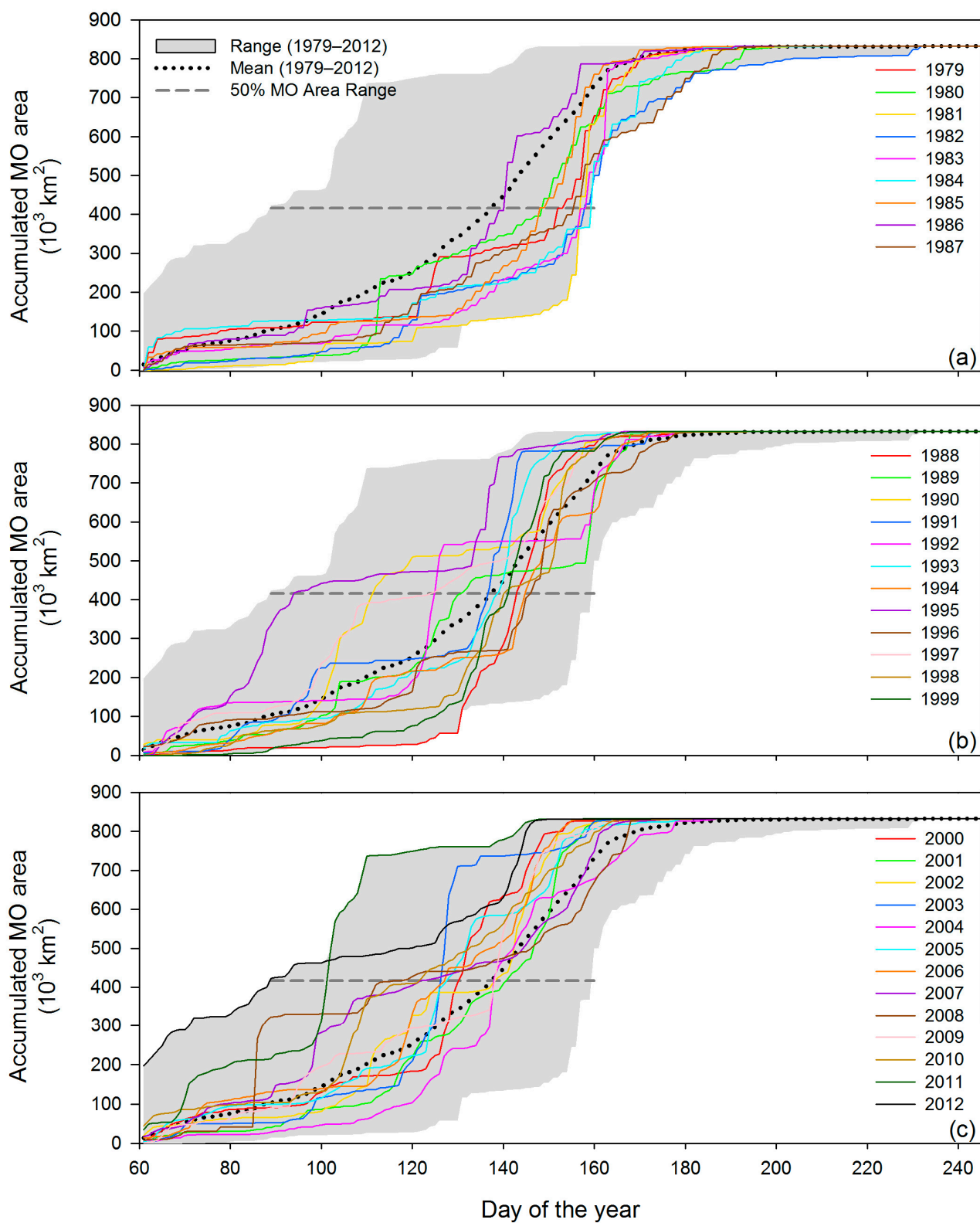


Figure 10. Laptev Sea annual accumulated MO areas for (a) SMMR years; (b) early SSM/I years; and (c) late SSM/I and SSMIS years.

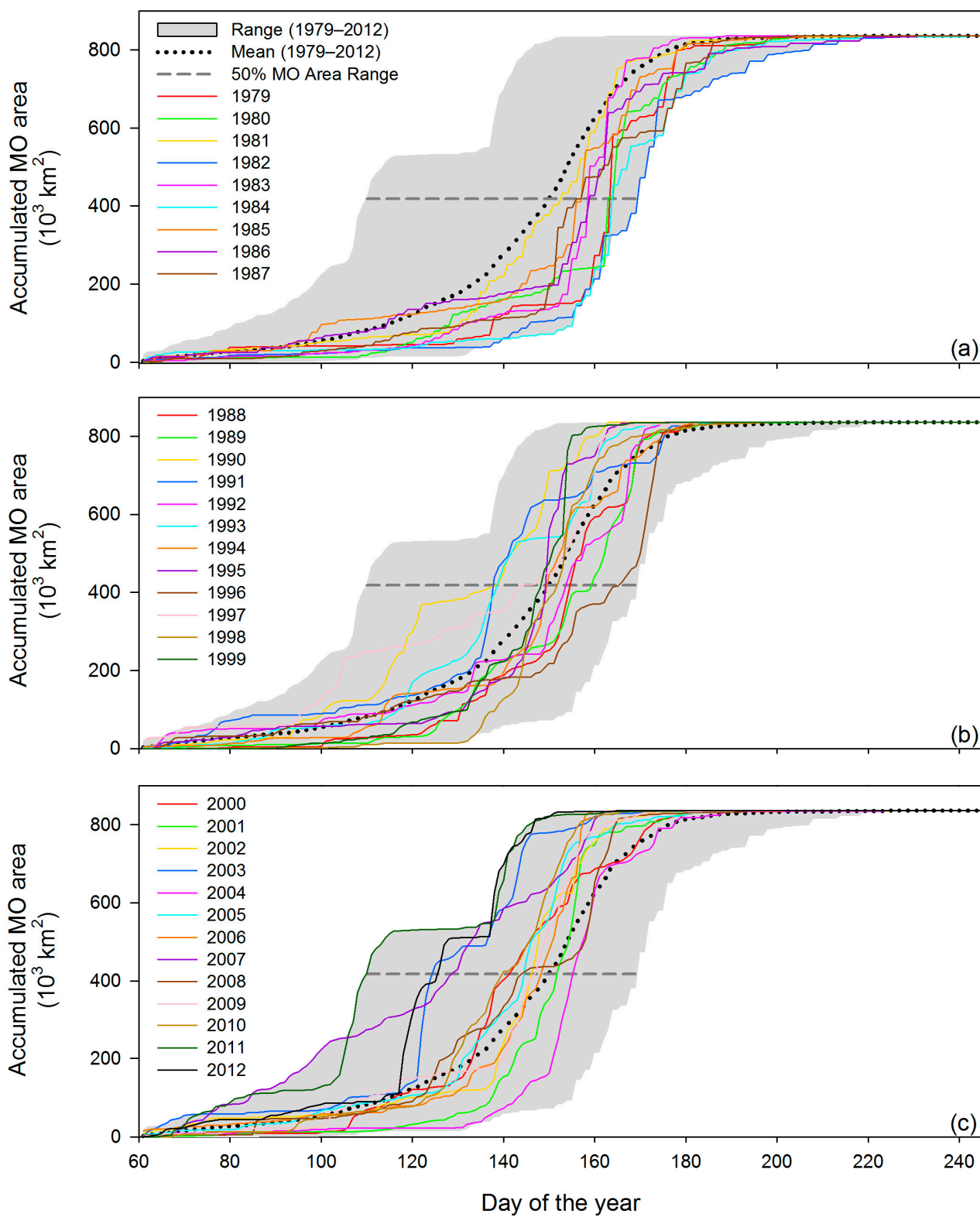


Figure 11. East Siberian Sea annual accumulated MO areas for (a) SMMR years; (b) early SSM/I years; and (c) late SSM/I and SSMIS years.

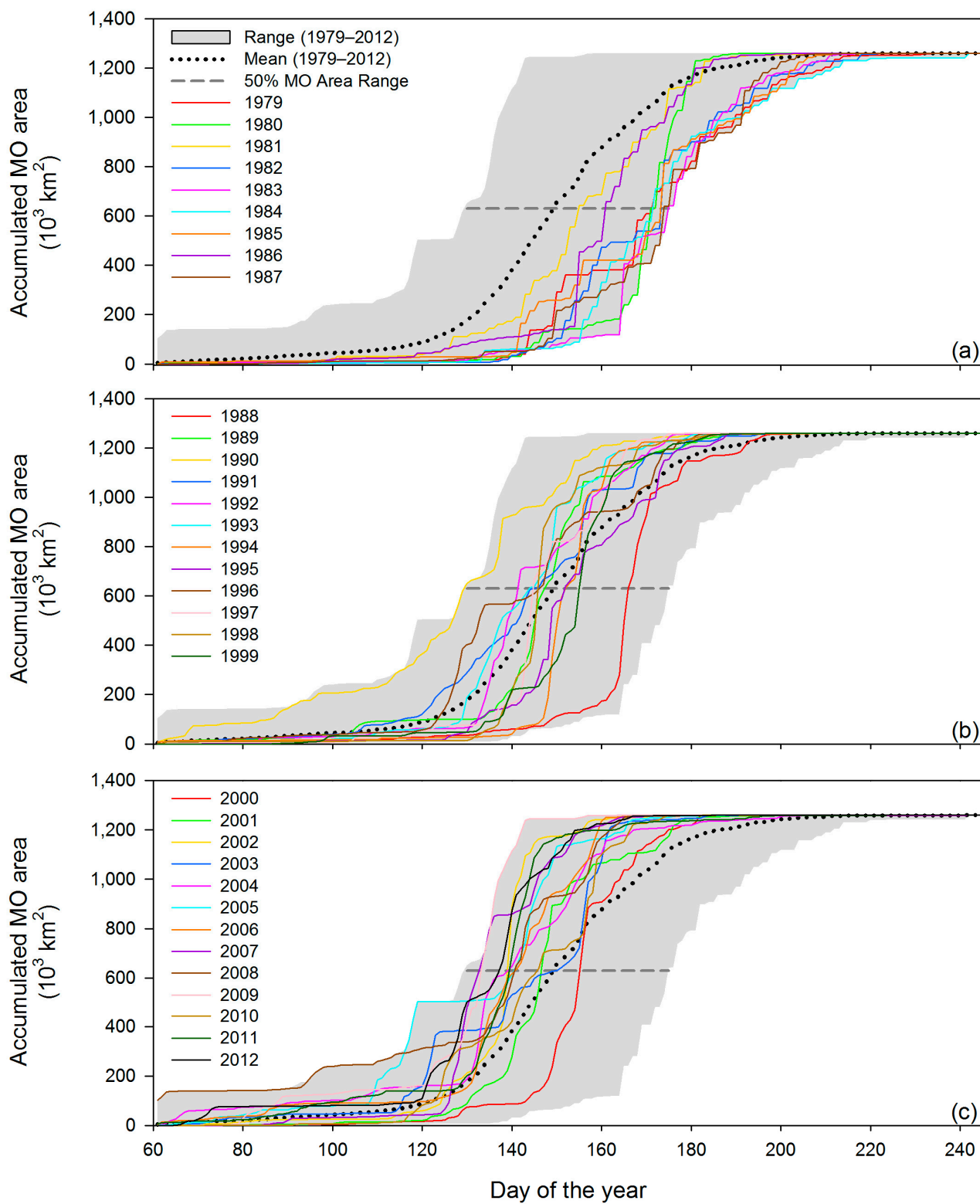


Figure 12. Chukchi Sea annual accumulated MO areas for (a) SMMR years; (b) early SSM/I years; and (c) late SSM/I and SSMIS years.

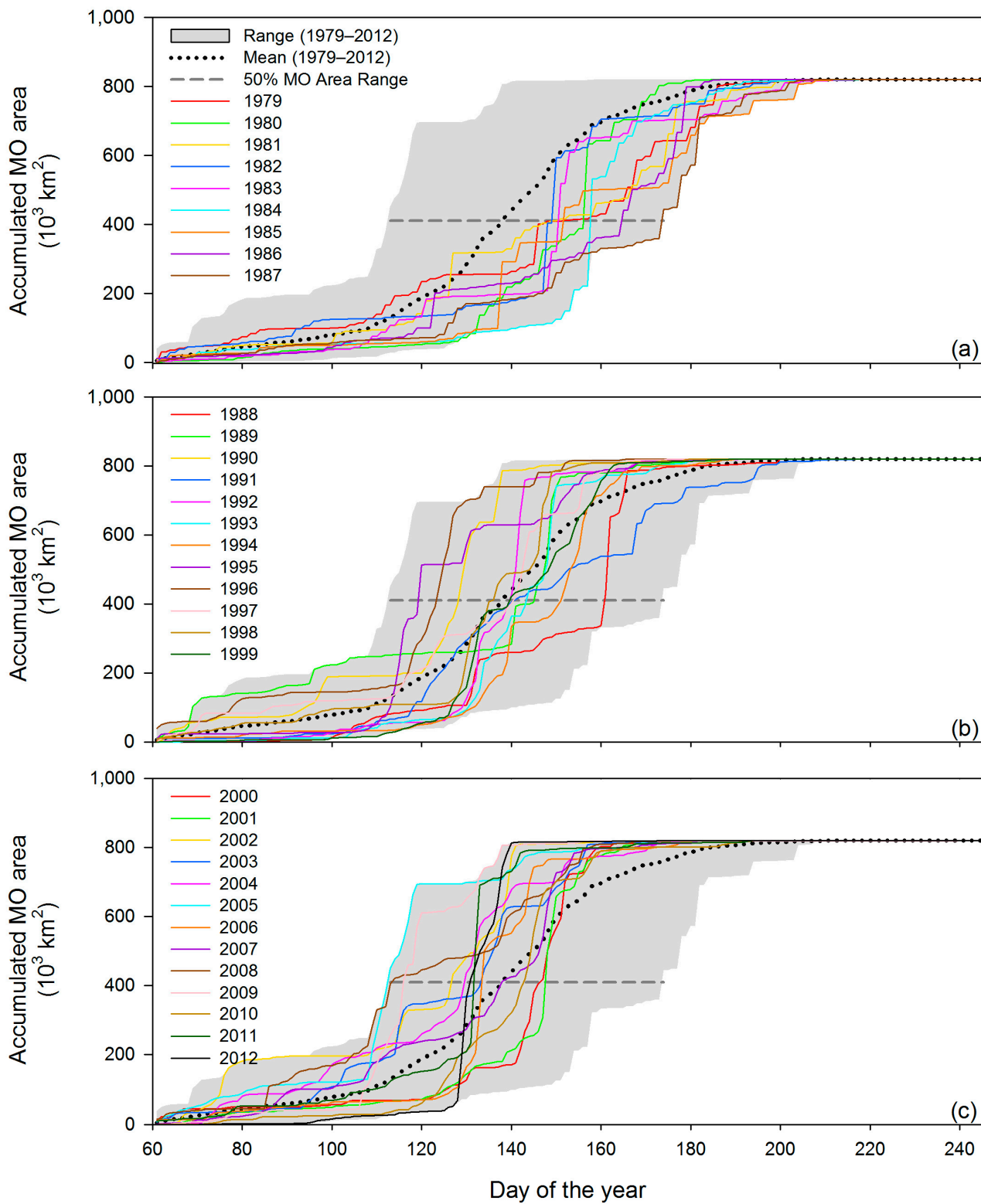


Figure 13. Beaufort Sea annual accumulated MO areas for (a) SMMR years; (b) early SSM/I years; and (c) late SSM/I and SSMIS years.

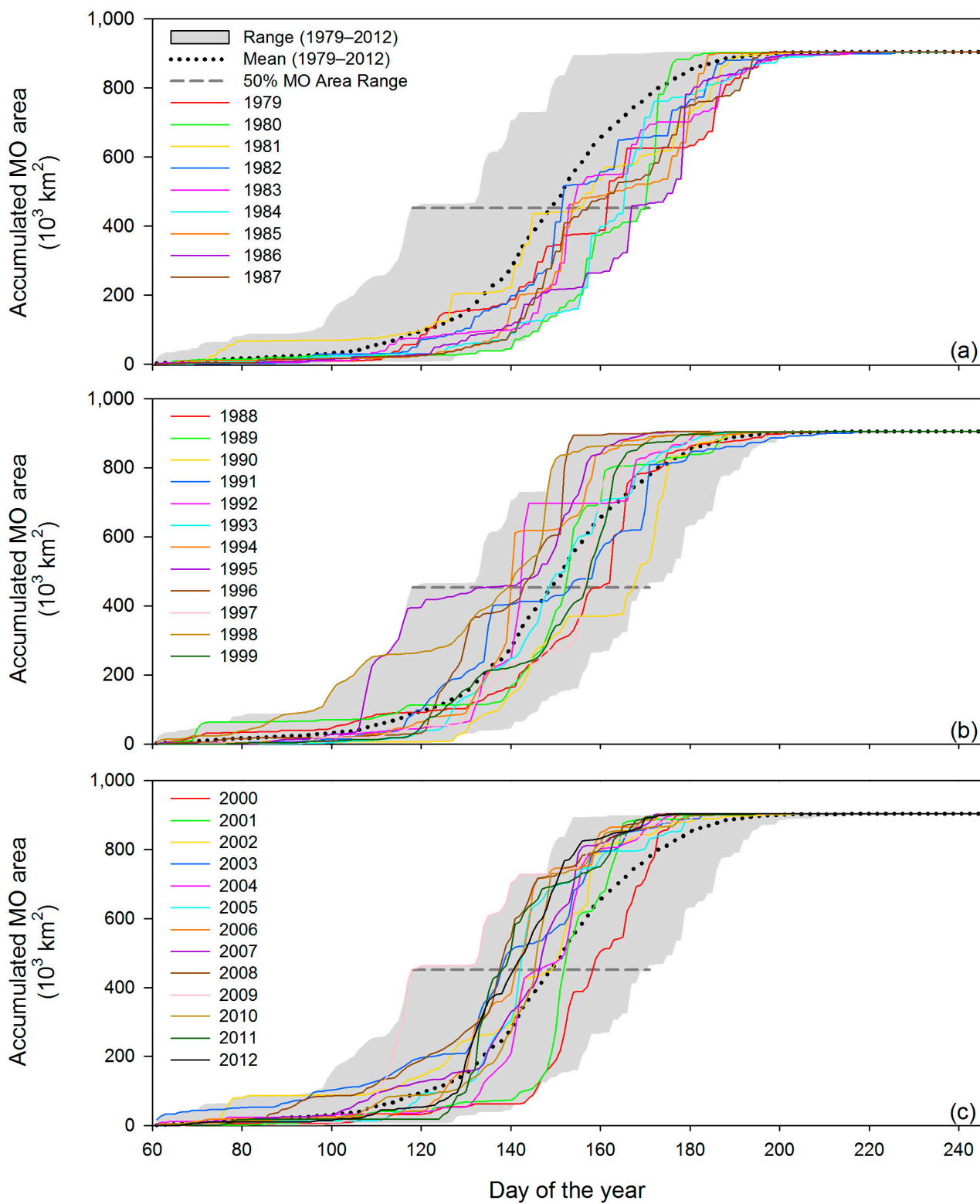


Figure 14. Canadian Arctic Archipelago annual accumulated MO areas for (a) SMMR years; (b) early SSM/I years; and (c) late SSM/I and SSMIS years.

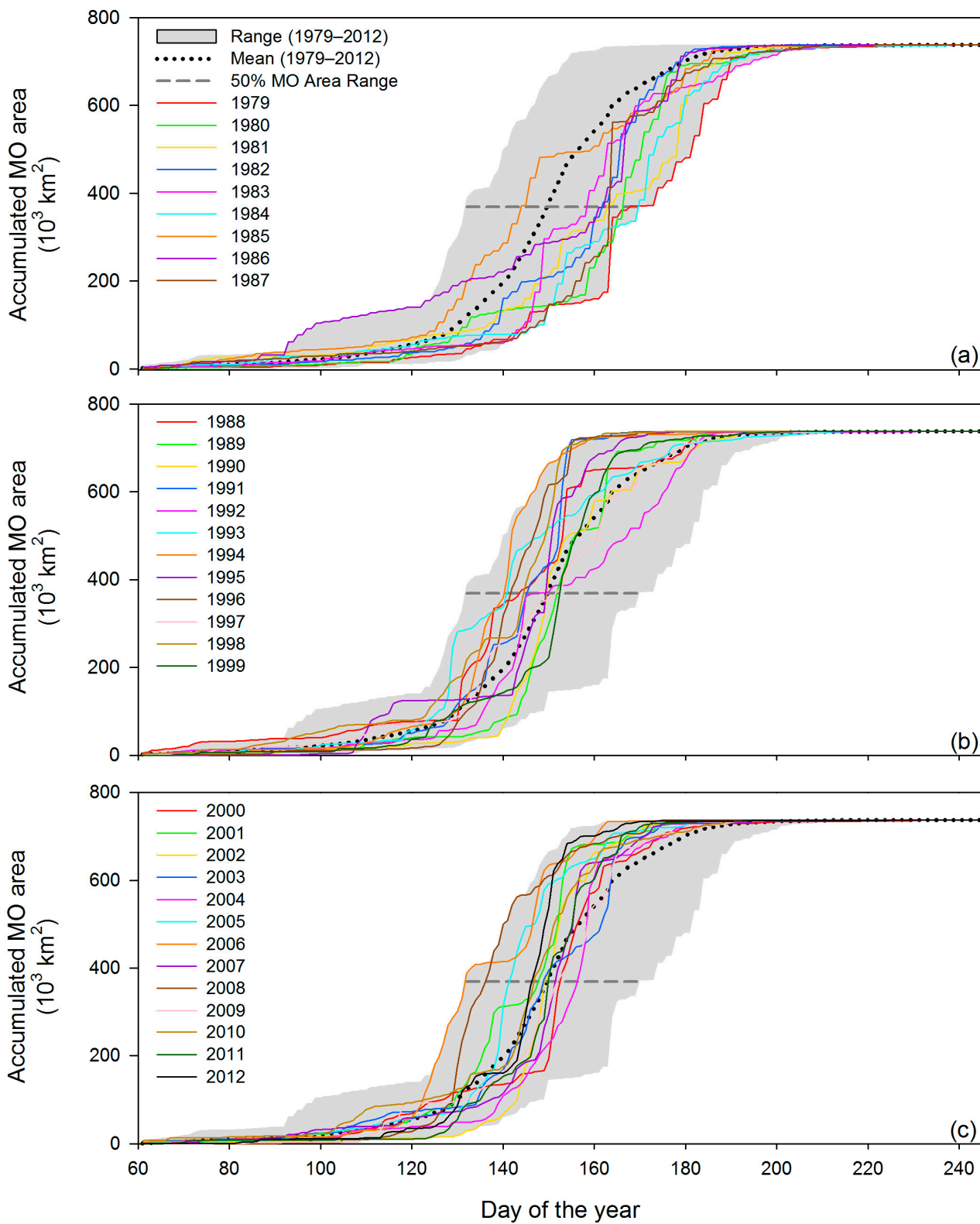


Figure 15. Central Arctic annual accumulated MO areas for (a) SMMR years; (b) early SSM/I years; and (c) late SSM/I and SSMIS years.

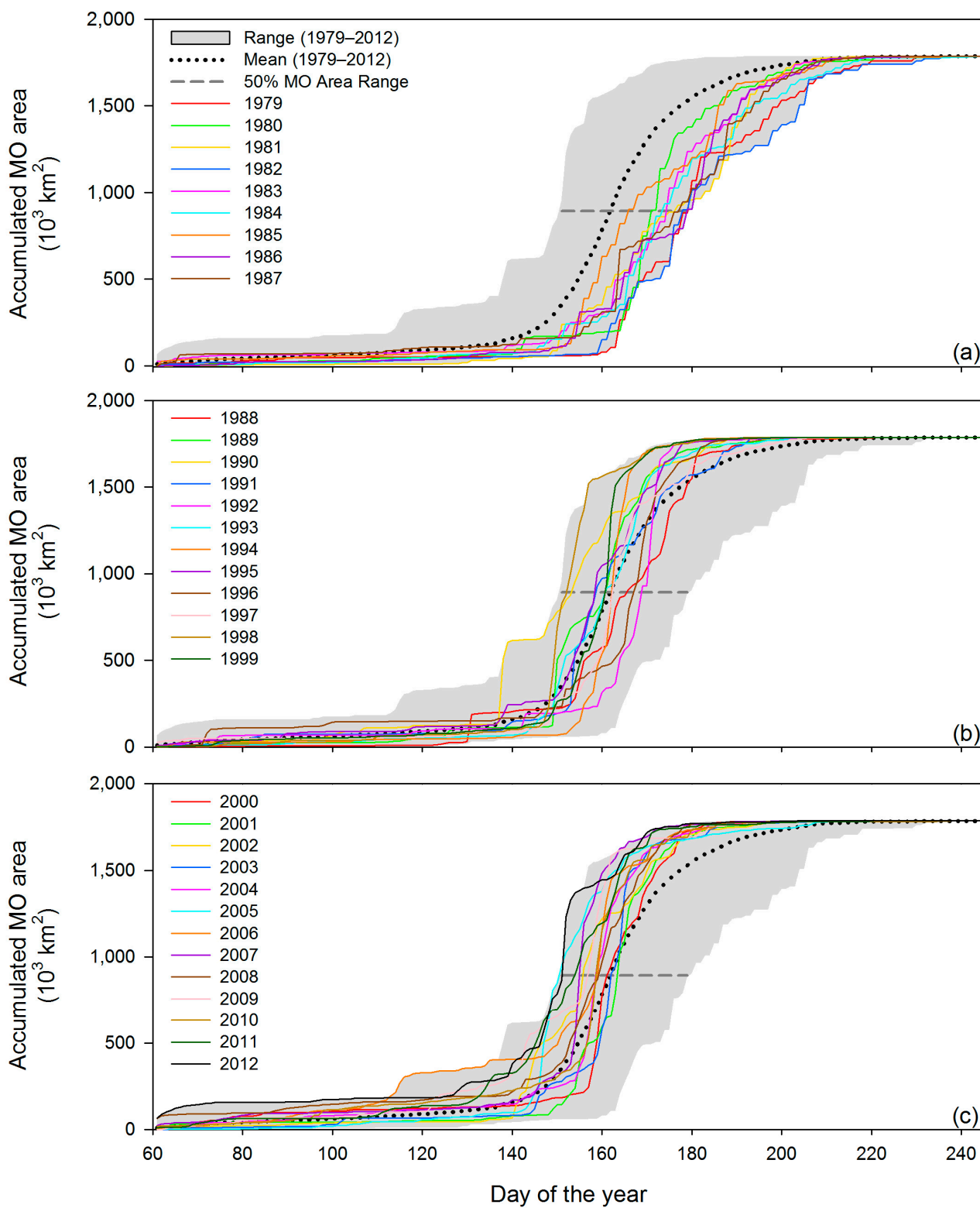


Figure 16. Baffin Bay annual accumulated MO areas for (a) SMMR years; (b) early SSM/I years; and (c) late SSM/I and SSMIS years.

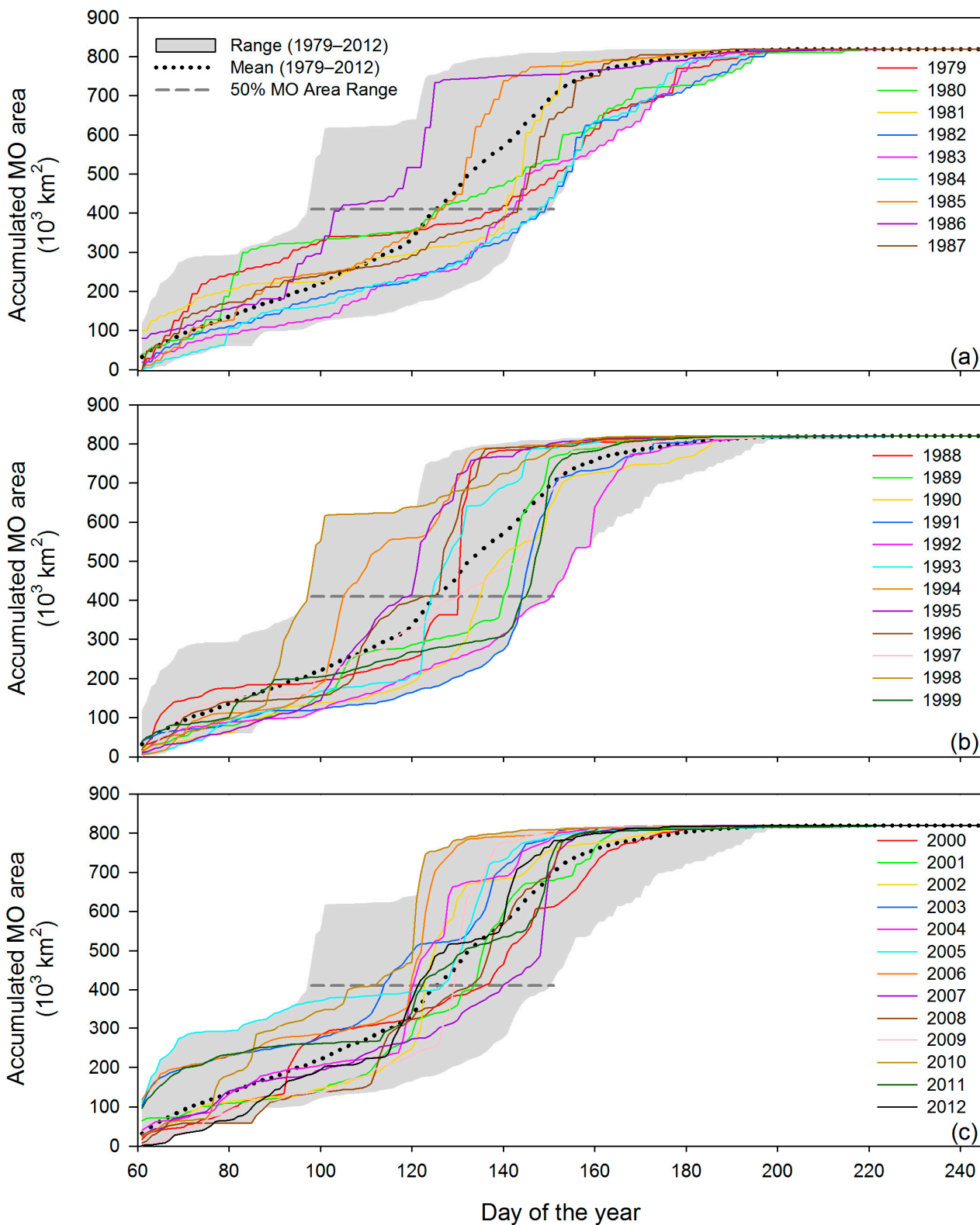
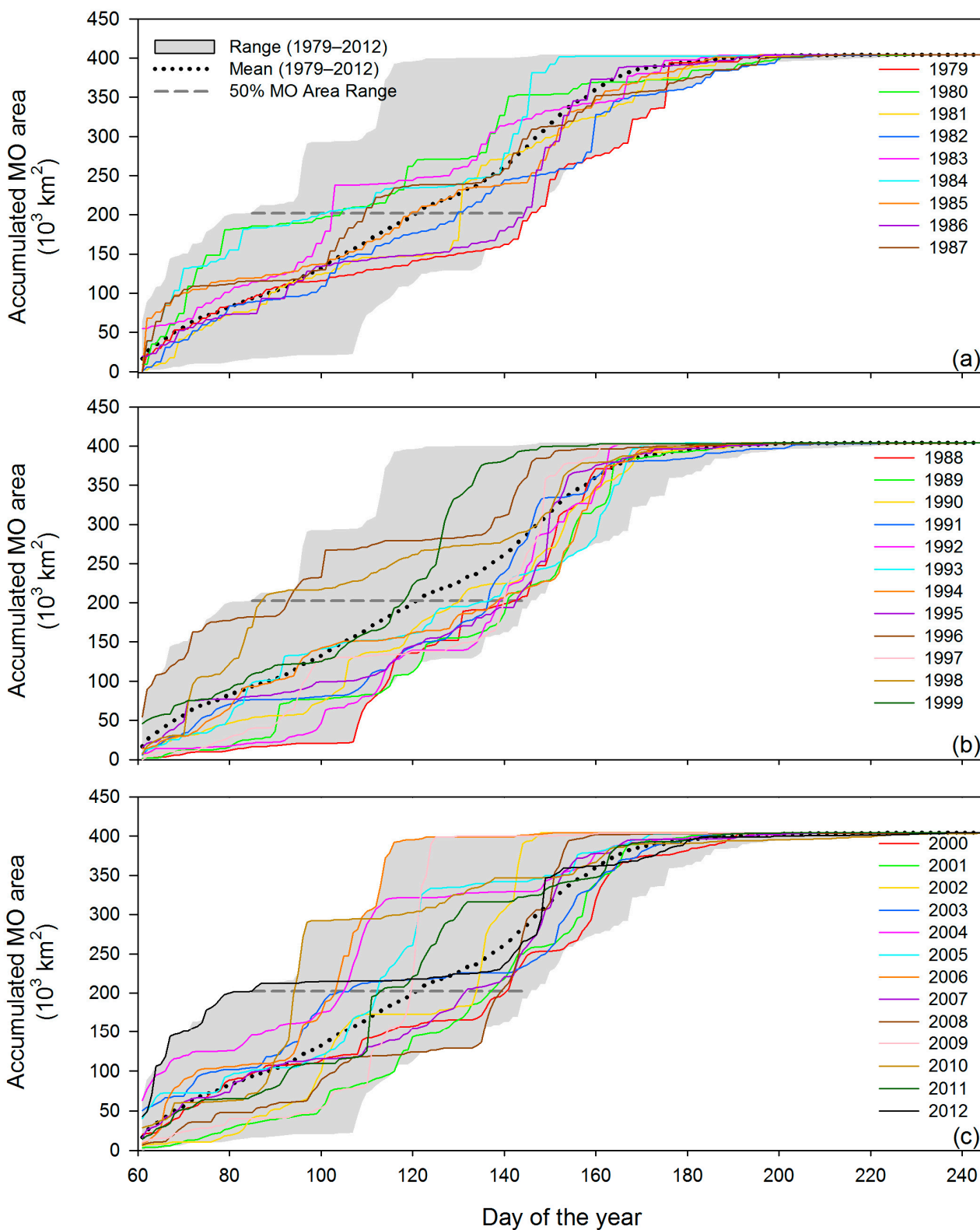


Figure 17. Greenland Sea annual accumulated MO areas for (a) SMMR years; (b) early SSM/I years; and (c) late SSM/I and SSMIS years.



The pattern in the range of MO area accumulations differs for each region. For example, the Central Arctic region surrounds the pole at the highest latitudes, excluding the “pole hole;” thus, the earliest MO area accumulations tend to begin later in the season than for regions at lower latitudes (Figure 15).

However, MO area accumulates more rapidly here than for other regions; that is, the slope of the accumulation curve is much steeper over the length of the MO period than compared to other regions such as the Barents, Kara, Laptev, East Siberian, Chukchi, Beaufort, and Greenland Seas as well as Baffin Bay (Figures 8–13,15–17). This result corresponds to the findings of Wang *et al.* [8], which describe a fast progression of melting in the horizontal direction in the Central Arctic, upwards of $60 \text{ km}\cdot\text{day}^{-1}$, likely due to the influence of cyclonic weather activity.

In general, the shift towards earlier accumulations of MO area in the Arctic Ocean (Figure 7) over the satellite record also appears to a varying degree in all sub-regions (Figures 8–17). MO area accumulations for most regions generally fall below the region's mean MO accumulation during the early part of the record (SMMR years), while MO accumulations in the early and late SSM/I years shift earlier in the year. In addition to the shift towards earlier MO for the study years, inter-annual variability within single sub-regions of the Arctic can be large. There are cases where anomalously early or late MO area accumulation years appear clearly within each region. An example of very high inter-annual variability occurs in the East Siberian Sea in 1990 (an early MO area accumulation year) and 1988 (a late MO area accumulation year) which both occurred during the early SSM/I years (Figure 11b).

To compare the degree of variability from year to year in MO area accumulations for each region, the range of 50% MO area days is used (Table 2). We define this value as the difference between the earliest date and latest date on which 50% of the region's total area had experienced MO for the 34 years in the record. This range (hereafter 50% MO area range) corresponds to the horizontal width of the grey shaded regions shown in Figures 7–17 at 50% of the region's total area and is marked on each plot with a horizontal dashed line. We use the day of year on which 50% of the area for a region has experienced MO as a measure of the central point of the MO period in terms of area.

Table 2. Range and mean date on which 50% MO area occurred 1979–2012.

Region	50% MO Area Range (Days)	Mean 50% MO Area Date (DOY)
Arctic Ocean	30	148.8
Barents Sea	61	88.6
Kara Sea	71	134.8
Laptev Sea	60	148.6
East Siberian Sea	45	151.4
Chukchi Sea	61	140.9
Beaufort Sea	53	149.9
Canadian Archipelago	38	151.2
Central Arctic	28	163.7
Baffin Bay	53	129.7
Greenland Sea	60	122.6

The Kara Sea is the most highly variable region in MO area accumulation with a 71 day 50% MO area range (Table 2 and Figure 9). By comparison, the Arctic Ocean region, which includes MO dates for all sub-regions included in this study, has a 30 day 50% MO area range; again highlighting the importance of regional analysis. The Barents Sea (Figure 8), Laptev Sea (Figure 10), Chukchi Sea

(Figure 12), and Greenland Sea (Figure 17) are similar to the Kara Sea in that the 50% MO area range is about 60–61 days for the four regions (Table 2). Although the range is similar, the 50% MO area range in the Laptev Sea seems to be heavily influenced by two extremely early MO area accumulation years: 2007 and 2011 (Figure 10). In the Chukchi Sea, however, the variability of MO area accumulation curves is greater, and anomalous years such as in the Laptev Sea do not stand out against other years. This might indicate that, with the exception of extreme years, the Laptev Sea MO area accumulations are in general not as highly variable as the MO accumulations in the Chukchi Sea as the similar 50% MO area ranges might suggest.

Although there is an overall shift towards earlier MO for much of the Arctic sea ice cover, the high variability from year to year in individual sub-regions, gives evidence that the timing and magnitude of MO area accumulations are still highly dependent on the atmospheric conditions present at the time of MO in a particular region. Anderson and Drobot [18] have shown that the MO dates in one region of the Arctic are largely independent of the MO dates in other regions. This is most likely due to the regional nature of cyclonic activity and the associated warm air anomalies [13,19] and increased longwave radiation flux at the surface due to enhanced cloud cover (e.g., [36,37]). Therefore, an extreme MO area accumulation (one that is at either the early or late ends of the 50% MO area range) in a region one year may not appear to be an abnormal year for other regions. For example, the MO area accumulation is extremely early for 1990 in the East Siberian Sea (Figure 11b) and also shows up as an early MO accumulation year for the Kara, Laptev, Chukchi, and for at least a portion of the Central Arctic region (Figure 9b,10b,12b,15b). However, 1990 MO area accumulation occurs later in the year than the mean for the Beaufort Sea and the Canadian Arctic Archipelago (Figure 13b,14b). 1990 is an anomalous year in terms of MO area because this year is associated with a strongly positive AO Index in the winter and the early spring [19]. The positive AO Index was found to be associated with earlier snow melt onset in the Laptev, East Siberian, and Chukchi Sea regions. Since MO is so closely tied to the cyclonic-scale weather conditions, variations in the MO area accumulations from year to year reflect the variability of spring weather. Although out of the scope of this paper, it is clear from the significant changes in MO area accumulations that the weather conditions and timing of melt forcing have changed over the study period (1979–2012).

7. Summary and Conclusions

The present study examines the variability in the timing of areal accumulations of MO on Arctic Ocean sea ice through 1979–2012 melt seasons. The timing of MO in a particular location is tied to the atmospheric conditions present at the time of melting, resulting in air temperatures reaching the freezing point. In all regions of the Arctic Ocean, MO area has been accumulating increasingly earlier in the year. The increasingly early snow MO over much of the Arctic contributes to increased radiation absorption over an already vulnerable, thin sea ice cover. Although the general tendency is for increasingly early MO in the Arctic Ocean region, there is high regional and inter-annual variability indicative of the close association between MO and weather variability during the Arctic spring. Various patterns appear in the timing of daily MO area over individual melt seasons. In some cases, MO area accumulates slowly over a long period of time. In other cases, large areas experience MO over a short 3–5 day time period. In both of these melt event types the location and track of cyclonic activity can

influence the degree to which MO area accumulates over a time period. The influence of a cyclone on the air temperatures and cyclonic winds increasing the air temperature via warm air advection from the south can be a mechanism leading to these intense, short duration melting events such as occurs in the Kara Sea during 1992. While slower, long duration melting events such as occurs in the Kara Sea during 1985 are generally associated with relatively high mean sea level pressures and relatively cooler temperatures, possibly delaying the accumulation of large MO area despite the seasonal warming of air temperatures into the late spring and summer. The net effects of these different types of melting events may produce similar total melt areas, but an intense melt event earlier in the year can have a greater impact on the net surface energy budget in the region for the given season than a slower accumulation of MO area.

Additionally, the temporal scale of intense melt events which occur over a 3–5 day period, gained by analyzing the MO patterns on a day-by-day basis illustrates the necessity for further investigation into the relationship between synoptic-scale weather and whether or not MO will occur anomalously early in a region. The overall trend towards increasingly early MO in the Arctic is related to warming temperatures in the Arctic; however, the high regional and inter-annual variability and susceptibility of the sea ice to episodic events and sensitivity to individual cyclonic events warrants further analysis to determine how these smaller scale (spatial and temporal) events contribute to ongoing changes in sea ice.

Acknowledgments

This work was partially supported by NASA grants [NNG04GG85G] and [NNX08AP34A_S02] and NOAA grant [NA08OAR4310677]. The authors thank three anonymous reviewers for providing constructive feedback on this work and acknowledge the NOAA/ESRL Physical Sciences Division, Boulder Colorado for providing images used in Figures 4 and 6.

Author Contributions

Angela C. Bliss wrote the initial draft of this paper with input and editing by Mark R. Anderson. Mark R. Anderson provided the data processing to calculate areas of MO onset and collaborated with Angela C. Bliss on the development of the daily MO area time series and MO accumulation figures. Angela C. Bliss created the maps for Figures 1, 3 and 5, calculated the statistics presented in this paper.

Conflicts of Interest

The authors declare no conflicts of interest.

References

1. Parkinson, C.L.; Comiso, J.C. On the 2012 record low arctic sea ice cover: Combined impact of preconditioning and an August storm. *Geophys. Res. Lett.* **2013**, *40*, 1356–1361.
2. Comiso, J.C.; Parkinson, C.L.; Gersten, R.; Stock, L. Accelerated decline in the arctic sea ice cover. *Geophys. Res. Lett.* **2008**, *35*, doi:10.1029/2007GL031972.

3. Kwok, R.; Cunningham, G.F.; Wensnahan, M.; Rigor, I.; Zwally, H.J.; Yi, D. Thinning and volume loss of the arctic ocean sea ice cover: 2003–2008. *J. Geophys. Res.* **2009**, *114*, doi:10.1029/2009JC005312.
4. Nghiem, S.V.; Rigor, I.G.; Perovich, D.K.; Clemente-Colón, P.; Weatherly, J.W.; Neumann, G. Rapid reduction of arctic perennial sea ice. *Geophys. Res. Lett.* **2007**, *34*, doi:10.1029/2007GL031138.
5. Lindsay, R.W.; Zhang, J.; Schweiger, A.; Steele, M.; Stern, H. Arctic sea ice retreat in 2007 follows thinning trend. *J. Clim.* **2009**, *22*, 165–176.
6. Ogi, M.; Wallace, J.M. Summer minimum arctic sea ice extent and the associated summer atmospheric circulation. *Geophys. Res. Lett.* **2007**, *34*, doi:10.1029/2007GL029897.
7. Simmonds, I.; Rudeva, I. The great arctic cyclone of August 2012. *Geophys. Res. Lett.* **2012**, *39*, doi:10.1029/2012GL054259.
8. Wang, L.; Wolken, G.J.; Sharp, M.J.; Howell, S.E.L.; Derksen, C.; Brown, R.D.; Markus, T.; Cole, J. Integrated pan-arctic melt onset detection from satellite active and passive microwave measurements, 2000–2009. *J. Geophys. Res.* **2011**, *116*, doi:10.1029/2011JD016256.
9. Curry, J.A.; Schramm, J.L.; Ebert, E.E. Sea ice-albedo climate feedback mechanism. *J. Clim.* **1995**, *8*, 240–247.
10. Perovich, D.K.; Nghiem, S.V.; Markus, T.; Schweiger, A. Seasonal evolution and interannual variability of the local solar energy absorbed by the arctic sea ice—Ocean system. *J. Geophys. Res.* **2007**, *112*, doi:10.1029/2006JC003558.
11. Perovich, D.K.; Polashenski, C. Albedo evolution of seasonal arctic sea ice. *Geophys. Res. Lett.* **2012**, *39*, doi:10.1029/2012GL051432.
12. Stroeve, J.C.; Markus, T.; Boisvert, L.; Miller, J.; Barrett, A. Changes in arctic melt season and implications for sea ice loss. *Geophys. Res. Lett.* **2014**, *41*, doi:10.1002/2013GL058951.
13. Belchansky, G.I.; Douglas, D.C.; Platonov, N.G. Duration of the arctic sea ice melt season: Regional and interannual variability 1979–2001. *J. Clim.* **2004**, *17*, 67–80.
14. Markus, T.; Stroeve, J.C.; Miller, J. Recent changes in arctic sea ice melt onset, freezeup, and melt season length. *J. Geophys. Res.* **2009**, *114*, doi:10.1029/2009JC005436.
15. Drobot, S.D.; Anderson, M.R. An improved method for determining snowmelt onset dates over arctic sea ice using scanning multichannel microwave radiometer and special sensor microwave/imager data. *J. Geophys. Res.* **2001**, *106*, 24033–24049.
16. Smith, D.M. Observation of perennial arctic sea ice melt and freeze-up using passive microwave data. *J. Geophys. Res.* **1998**, *3*, 27753–27769.
17. Anderson, M.R. Snow melt on sea ice surfaces as determined from passive microwave satellite data. In *Large Scale Effects of Seasonal Snow Cover*, Proceedings of an International Symposium Held During the XIXth General Assembly of the International Union of Geodesy and Geophysics, Vancouver, BC, Canada, 9–22 August 1987; pp. 329–342.
18. Anderson, M.R.; Drobot, S.D. Spatial and temporal variability in snowmelt onset over arctic sea ice. *Ann. Glaciol.* **2001**, *33*, 74–78.
19. Drobot, S.D.; Anderson, M.R. Comparison of interannual snowmelt-onset dates with atmospheric conditions. *Ann. Glaciol.* **2001**, *33*, 79–84.

20. Serreze, M.C.; Maslanik, J.A.; Key, J.R.; Kokaly, R.F.; Robinson, D.A. Diagnosis of the record minimum in arctic sea ice area during 1990 and associated snow cover extremes. *Geophys. Res. Lett.* **1995**, *22*, 2183–2186.
21. Bliss, A.C.; Anderson, M.R. Daily accumulated area of snow melt onset on arctic sea ice. In Proceedings of the American Geophysical Union fall meeting, San Francisco, CA, USA, 3–7 December 2012.
22. Anderson, M.R.; Bliss, A.C.; Drobot, S.D. *Snow Melt Onset over Arctic Sea Ice from SMMR and SSM/I-SSMIS Brightness Temperatures*, Version 3.0 (1979–2012); NASA DAAC at the National Snow and Ice Data Center: Boulder, CO, USA, 2014.
23. National Snow and Ice Data Center. Documentation: Polar Stereographic Projection and Grid. Available online: https://nsidc.org/data/polar_stereo/ps_grids.html (accessed on 28 March 2014).
24. Stroeve, J.; Maslanik, J.; Li, X. An intercomparison of DMSP F11- and F13-Derived sea ice products. *Remote Sens. Environ.* **1998**, *64*, 132–152.
25. Abdalati, W.; Steffen, K.; Otto, C.; Jezek, K.C. Comparison of brightness temperatures from SSMI instruments on the DMSP F8 and F11 satellites for Antarctica and the Greenland ice sheet. *Int. J. Remote Sens.* **1995**, *16*, 1223–1229.
26. Jezek, K.C.; Merry, C.; Cavalieri, D.; Grace, S.; Bedner, J.; Wilson, D.; Lampkin, D. *Comparison Between SMMR and SSM/I Passive Microwave Data Collected Over the Antarctic Ice Sheet*; Byrd Polar Research Center Technical Report, no. 91–03; The Ohio State University: Columbus, OH, USA, 1991.
27. Meier, W. (NASA Goddard Space Flight Center Cryospheric Sciences Laboratory, Greenbelt, MD, USA). Provided correlation coefficients derived from data DMSP F13–F17 satellite overlap periods to adjust passive microwave brightness temperatures used in the calculation of melt onset dates, 2011.
28. Livingstone, C.E.; Singh, K.P.; Gray, L. Seasonal and regional variations of active/passive microwave signatures of sea ice. *IEEE Trans. Geosci. Remote Sens.* **1987**, *GE-25*, 159–172.
29. Meier, W.N.; Stroeve, J.; Fetterer, F. Wither arctic sea ice? A clear signal of decline regionally, seasonally and extending beyond the satellite record. *Ann. Glaciol.* **2007**, *46*, 428–434.
30. Parkinson, C.L.; Cavalieri, D.J.; Gloersen, P.; Zwally, H.J.; Comiso, J.C. Arctic sea ice extents, areas, and trends, 1978–1996. *J. Geophys. Res.* **1999**, *104*, 20837–20856.
31. Kalnay, E.; Kanamitsu, M.; Kistler, R.; Collins, W.; Deaven, D.; Gandin, L.; Iredell, M.; Saha, S.; White, G.; Woollen, J.; *et al.* The NCEP/NCAR 40-year reanalysis project. *Bull. Am. Meteor. Soc.* **1996**, *77*, 437–471.
32. The NCEP/NCAR Reanalysis Project at the NOAA/ESRL Physical Sciences Division. Available online: <http://www.esrl.noaa.gov/psd/> (accessed on 3 October 2014).
33. Screen, J.A.; Simmonds, I. The central role of diminishing sea ice in recent arctic temperature amplification. *Nature* **2010**, *464*, 1334–1337.
34. Serreze, M.C.; Barrett, A.P.; Stroeve, J.C.; Kindig, D.N.; Holland, M.M. The emergence of surface-based arctic amplification. *Cryosphere* **2009**, *3*, 11–19.
35. Serreze, M.C.; Francis, J.A. The arctic amplification debate. *Clim. Chang.* **2006**, *76*, 241–264.

36. Bennartz, R.; Shupe, M.D.; Turner, D.D.; Walden, V.P.; Steffen, K.; Cox, C.J.; Kulie, M.S.; Miller, N.B.; Pettersen, C. July 2012 Greenland melt extent enhanced by low-level liquid clouds. *Nature* **2013**, *496*, 83–86.
37. Crane, R.G.; Anderson, M.R. Springtime microwave emissivity changes in the southern Kara Sea. *J. Geophys. Res.* **1994**, *99*, 14303–14309.

© 2014 by the authors; licensee MDPI, Basel, Switzerland. This article is an open access article distributed under the terms and conditions of the Creative Commons Attribution license (<http://creativecommons.org/licenses/by/4.0/>).